NTNU
Norwegian University of
Science and Technology

Time-Lapse Refraction Analysis Monitoring Shallow Gas Migration

2/4-14 Blowout, A North Sea Case Study

Nora Løw Løhre

Petroleum Geoscience and Engineering
Submission date: June 2018
Supervisor: Martin Landrø, IGP

Norwegian University of Science and Technology
Department of Geoscience and Petroleum

Abstract

In January 1989, the drilling of well 2/4-14 situated in the North Sea took a dramatic turn of events when encountering a high-pressure zone. The well kicked and the situation eventually developed into an underground blowout. The blowout lasted for 326 intense days, and by drilling the relief well 2/4-15, the well was finally killed in December 1989. In close proximity to the well, a tunnel valley system is present. Due to the geology, structure, and infill of these kinds of systems, they have potential to act as excellent recipients and conduits for migrating gas. Repeated seismic has been acquired over this area from 1988 to 2009, providing a great potential for mapping and investigating the gas and its movements.

The study is a continuation of the specialization project *4D refraction time-shift analysis of a shallow subsurface gas flow*, with the aim to perform a time-lapse refraction analysis on three 2D surveys acquired in 1988, 1990 and 2009. Refractions primarily travel in the horizontal direction, in contrast to the more vertical travel path of reflections. The principle difference between these methods is that the offset for refractions is larger in relation to the depth of the interface aimed to be explored. Utilizing the horizontal energy to generate time-shifts show variations in velocity at shallow depths, that might not be detected with conventional reflection methods (Zadeh & Landrø, 2011).

Throughout this thesis, two refractions from three repeated surveys have been successfully processed and analyzed. The results show estimations of significant time-shift anomalies in close proximity to the blowout well and the tunnel valley system. Interpretations of gas from the blowout both migrating into the tunnel valley system and out of it within a time-span of 20 years has been made. This thesis demonstrates the potential 4D refraction time-shift methods can have as a complementary 4D analysis technique, showing its ability to detect changes in velocity in shallow subsurface layers, where conventional reflection seismic methods might be inadequate.

Sammendrag

I januar 1989 tok boringen av brønn 2/4-14 i Nordsjøen en dramatisk vending. Brønnen støtte på en høytrykksone og opplevde et kick. Situasjonen utviklet seg etter hvert til en undergrunns utblåsning som varte i 326 intense dager. Ved boring av avlastningsbrønnen 2/4-15 ble brønnen omsider stengt i desember 1989. I nærheten av brønnen eksisterer et tunneldalsystem. Denne type systemer gir et godt potensial til å fungere som mottakere og ledere av migrerende gass, som følge av deres type struktur og litologi. Repetert seismikk har blitt samlet inn over dette området i perioden 1988 til 2009, noe som gir et godt grunnlag for monitorering av gass og dens bevegelser.

Studien er en fortsettelse av spesialiseringsprosjektet *4D refraction time-shift analysis of a shallow subsurface gas flow*, med sikte på å utføre en tidsskift refraksjonsanalyse på tre 2D-undersøkelser fra 1988, 1990 og 2009. Refraksjoner forflytter seg hovedsakelig i horisontal retning, i motsetning til den mer vertikale bevegelsen til refleksjoner. Hovedforskjeller mellom disse metodene er at offset for refraksjoner er større i forhold til dypet på den aktuelle grenseflaten. Ved å bruke den horisontale energien til å estimere tidsskift viser variasjoner i hastighet på grunnere dyp enn det som kanskje kan oppdages med konvensjonelle refleksjonsmetoder (Zadeh & Landrø, 2011).

Oppgaven tar for seg to refraksjoner fra tre repeterte seismiske undersøkelser, som her prosesseres og analyseres. Resultatene viser estimater av signifikante tidsskiftanomalier i nærheten av utblåsningsbrønnen og tunneldalsystemet. Det er blitt tolket at gass fra utblåsningen både migrerer inn i tunneldalsystemet of ut av det over en tidsperiode på 20 år. Denne oppgaven viser hvordan tidsskift av toveisgangtid kan brukes som en komplementær metode til 4D analyseteknikk, og evnen den har til å oppdage hastighetsendringer på grunne dyp, hvor konvensjonell refleksjonsseismikk ikke nødvendigvis strekker til.

Preface

This Master's thesis was written by Nora Løw Løhre during the spring of 2018. It marks the completion of a five-year study program leading to a M.Sc. in Petroleum Geosciences at the Norwegian University of Science and Technology (NTNU).

The thesis investigates how velocity changes can be detected and monitored in the shallower layers of the subsurface by analyzing time-shifts for time-lapse refraction seismic and is a continuation of the specialization project *4D Refraction Time-shift Analysis of a Shallow Subsurface Gas Flow – A case study from the North Sea* written the fall of 2017. The topic has been defined together with professor Martin Landrø.

My appreciation goes to my thesis advisor, Martin Landrø, whom I thank for his helpful guidance and inspiration, and for offering me the opportunity to partake in this interesting research area. Bjarte Foseide is also kindly thanked for his valuable input and technical assistance in addressing my task at hand. I would also like to thank Equinor for providing the seismic data used in this thesis.

Nora Løw Løhre

Trondheim, June 2018

Contents

List of Figures

1 Introduction

1.1 Background and Motivation

Almost three decades have passed since the dramatic incidence during drilling of well 14 in block 2/4. In January of 1989, the Saga Petroleum operated exploration well 2/4-14 experienced a kick at 4734 meters depth. After several attempts to regain control of the well, the drill pipe was cut, and the situation developed into an underground blowout. By the drilling of a relief well, the blowout was finally killed in December 1989.

On average, it was estimated that approximately 7800 b/d of oil and gas flowed uncontrollably into the subsurface. Immediately after the blowout, the rate was probably over 20 000 b/d (Landrø M. , 2011). The hydrocarbons migrated into shallower sand layers in the area, which is clearly visible on the seismic data. Most of the gas migrated to sand layers at 840 m, as well as into thin layers at approximately 490 m and 445 m. Nevertheless, it is likely that some gas has migrated into a tunnel valley system present at shallower depths. The area has been closely monitored, due to the risk the situation may impose. The blowout launched what probably is the first 4D seismic project on the Norwegian shelf, by acquiring high-resolution seismic data in an attempt to monitor the movement of escaped hydrocarbons over time (Landrø M. , 2011).

Seismic surveys were acquired frequently from 1988 until 1993. In 2009 Statoil repeated some of the 2D lines that were acquired 20 years earlier for research purposes. The repeatability of the data is relatively good and thus provides good opportunities for 4D seismic analysis. However, there are limitations in reflection seismic, and all details are not necessarily visible by the use of conventional reflection seismic methods. The objective of this project was to use time-lapse refraction seismic to monitor the gas migration from the underground blowout to as shallow depths as possible.

Monitoring how fluids migrate in the shallower subsurface is of great interest. Shallow gas can be considered as a geohazard and may impose a risk to installations, crew as well as the environment (Foseide, 2017). In this case, it is also of interest considering gas leakage to the water layer. Developing monitoring methods for studying shallow gas is also of great relevance when considering different carbon capture and storage scenarios.

This thesis is a continuation of the specialization project, written the fall of 2017. The objective of the project was to perform a 4D time-shift refraction analysis on a base and monitor survey,

acquired before and after the described blowout, to identify changes in velocity. The results showed clear indications of anomalies at shallow depths, which were interpreted to be gas from the blowout migrating into the tunnel valley system. By utilizing the repeated seismic from 2009, the continued migration of the gas can be investigated.

1.2 Goal and Method

This thesis was inspired by the research done by Anita Bjerkvik and Hossein Zadeh. The specialization project produced results that could be linked to the tunnel valley system. The goal for this thesis is to identify and monitor anomalies by correlating the results with the data from the 2009 survey to look for consistencies with the interpretations and to monitor the movement of the gas.

The technique of using 4D time-shift refraction analysis to estimate changes or differences in velocity was first introduced by Landrø et al. (2004). The approach was based on the idea of monitoring the changes in critical angle due to changes in velocity within a reservoir. This study demonstrated the potential refraction seismic methods could provide as a complementary monitoring method.

Methods using refraction seismic utilizes the waves that have been refracted at the critical angle. These types of waves are often termed as head waves or refractions. One of the main differences between reflected and refracted waves is the offset. To generate refractions larger offsets are needed in relation to the depth of the interface that is investigated. Hence, the travel path of refractions is primarily horizontal in contrast to the more vertical travel path of reflections. This enables the detection of variations in velocity that may not be visible on conventional reflection seismic (Zadeh & Landrø, 2011).

The results are generated by matching the datasets in geometry, followed by an alternation of base and monitor data. The time-shifts are then estimated by executing a standard windowed cross-correlation technique within a chosen offset range, for a specific refracted event. In this study, two refracted events are selected. One for larger offsets and a second refraction occurring at shorter offsets, close to 500 m.

2 Geology

2.1 Geological Setting

The area investigated throughout this study is block 2/4 located in the southern part of the Central North Sea, about 320 km southwest of Stavanger, Norway (Norwegian Petroleum Directorate, 2018). An overview of the North Sea and block 2/4 can be seen in Figure 2.1.1, where well 2/4-14 is marked in red. The Central North Sea is a basin set inland of the North Atlantic Margin, south of the Norwegian Sea (Anell, Thybo, & Rasmussen, 2007). Due to the relatively higher preservation factor in offshore sedimentation in the North Sea, an almost complete record of the sedimentation from the Cenozoic era is preserved. This provides detailed information on the geological history that has unfolded in this area. Due to the extensive exploration activities on the Norwegian shelf, the knowledge of the Cenozoic succession has significantly increased. Thus, detailed information about the geological history in the area of study is provided (Grindstad, 2017). The objective of this thesis limits the geology of interest to the shallow parts within the upper 1 km of the subsurface to be examined. This sequence is incorporated within the Nordland group as defined by Deegan and Scull (1977).

The Nordland group's geographical distribution spans from the western part of the Barents Sea to the southern part of the North Sea. It is present throughout the Mid-Norwegian shelf. The age of the group in this area ranges from Middle Miocene to present day (Norwegian Petroleum Directorate, 2018). Throughout the geological history of this area, the geology has been involved in dramatic changes. This includes periods of uplift, regressions, climatic cooling and periods of glacial activity. The depositional environment of the Nordland group is mainly open marine, with lithology dominated by marine claystones. These are grey in color, soft and locally silty and micaceous (Deegan & Scull, 1977). The lower part incorporates sandstone associated with the Utsira formation. The upper part of the group consists of unconsolidated sands and clay, overlain by an increasing content of glaciomarine deposits (NORLEX, 2018).

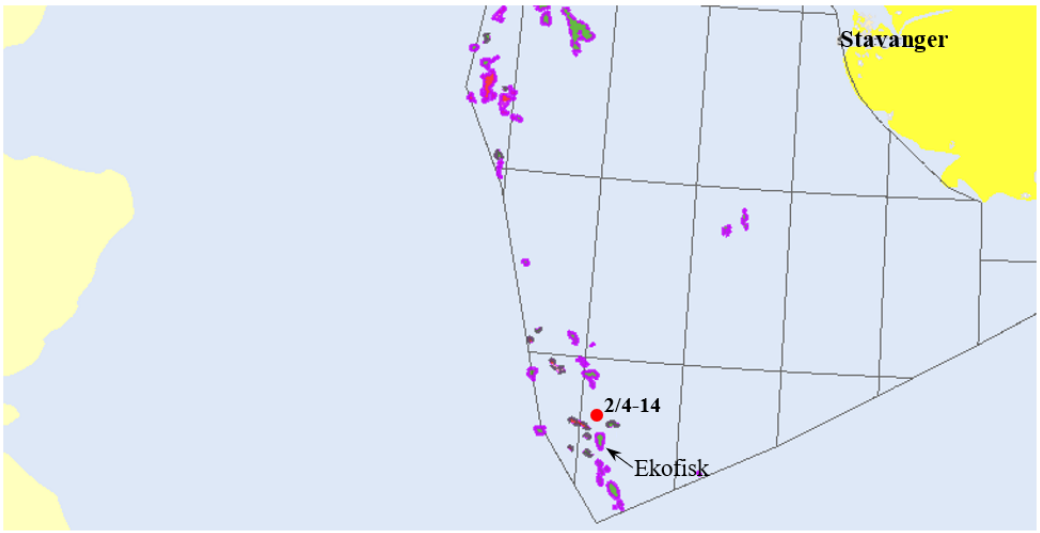

Figure 2.1.1: *Overview of the southern part of the North Sea. The location of well 2/4-14 is marked in red, the relief well 2/4-15 was drilled approximately 1 km south of this (NPD, 2018).*

2.2 Blowout in Well 2/4-14

In 1988, the drilling of a deep exploration well 2/4-14 started. The main area was the North Sea, in block 2/4 located in close proximity to the Ekofisk field (Norwegian Petroleum Directorate, 2018). The location of the well, in relation to Norway and the Ekofisk field, can be seen in Figure 2.1.1. The objective was to assess the hydrocarbon potential of the main structure (Norwegian Petroleum Directorate, 2018). The well was drilled into a rotated fault block of Late Jurassic age on the Steinbit Terrace. Saga Petroleum was the drilling operator, and the drilling of the well went without significant problems until January 1989, when the well encountered a high-pressure zone. At 4734 meters depth, the well kicked. The well was shut in, and several attempts were made to regain control, however unsuccessful. The blowout preventer (BOP) was closed, shear-rams were activated, and the drill pipe was cut on 20 January 1989 (Norwegian Petroleum Directorate, 2018). The situation escalated into an underground blowout (Mjelde & Bakøy, 1991). 11 days after blowout was declared, a relief well (Well 2/4-15) was spudded approximately 1.2 km south of well 2/4-14, in order to assist in the killing operations. Communication was reached by the two wells in December 1989, and the underground blowout was stopped by the injection of barite and mud of high density (Landrø M. , 2011). Finally, after 326 intense days, control was regained.

Saga Petroleum estimated that approximately 0.33 – 0.4 MSm^3 of oil and 196 – 367 MSm^3 of gas escaped from the reservoir and into shallower sand layers (Remen, 1991). According to

analysis done by Saga Petroleum, the major part of the hydrocarbons migrated into sand layers at approximately 840 m depth, and some gas also migrated into sand layers at 490 and 445 m (Landrø M. , 2011). The gas is clearly visible on the seismic data acquired from the area, as seen in Figure 2.2.1.

High-resolution seismic data was frequently acquired from 1988 to 1993. In addition, another site survey was acquired in 2009 by Statoil. The 2D lines repeated 20 years after the blowout can be seen in Figure 3.1.1. In this study, three seismic surveys acquired in 1988, 1990 and 2009 for line 804 intersecting the blowout well has been investigated.

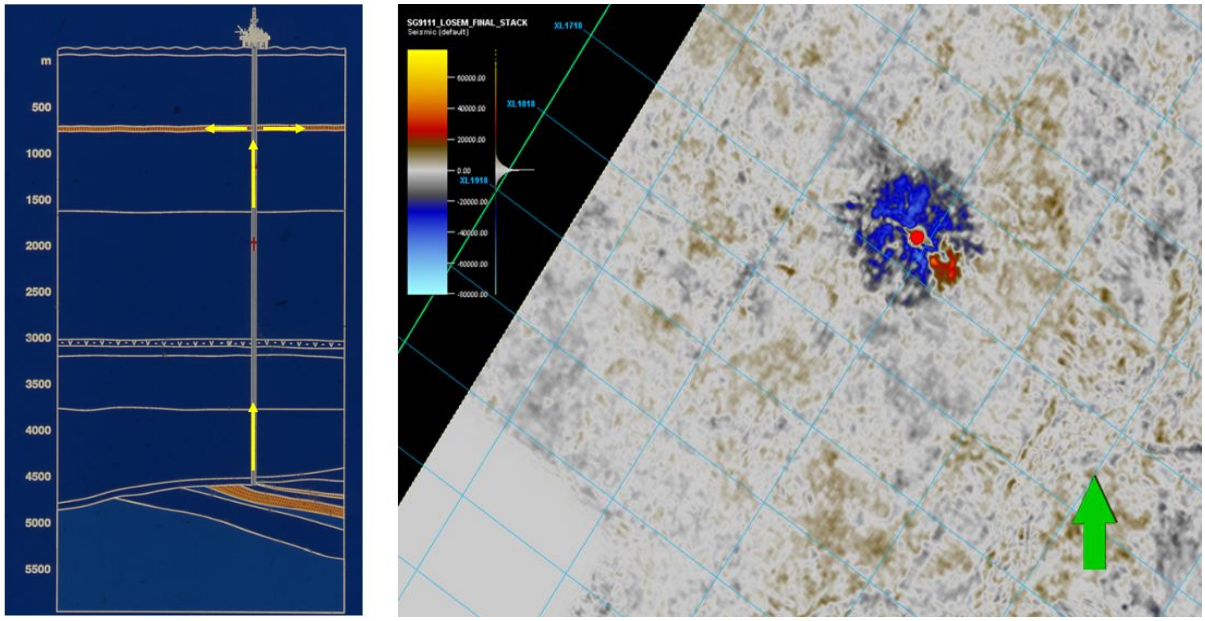

Figure 2.2.1*: To the left an illustration of well 2/4-14 showing target depth at approximately 4700 m. The yellow arrows demonstrate the hydrocarbon flow into the shallower sand layers (Landrø M. , 2011). To the right, hydrocarbons are clearly visible on the reflection seismic at 528 ms two-way travel time. The well is marked with a red circle.*

2.3 Tunnel Valley System

Tunnel valleys are defined as elongated depressions carved into deposited sediments or bedrocks during glaciations (Cofaigh, 1996). They often consist of several cut-and-fill structures, both in lateral and vertical direction. These structures form a network of interconnected valleys, which may occur as straight isolated valleys or more sinuous in shape. They are often characterized by steep dipping sides and floors that are highly irregular, and they commonly arrange anastomosing patterns (Cofaigh, 1996). The infill of these kinds of systems

may vary, but it is commonly dominated by units of sediments from glaciofluvial sands and gravity flows, hence the material is often coarse-grained and porous.

Several theories about the formation of tunnel valleys have been suggested. Still, there exists a sort of consensus that the valleys have been created during glacial or interglacial cycles, and are thus often a product of glacial drainage (Halvorsen, 2012). In the North Sea, the study area was mid-latitude and low-relief during the past glaciations. In flat terrain, it is unlikely to have large subglacial lakes present for long periods of time. To prevent large-scale surge and an eventual ice sheet collapse, the ice sheets may have turned to an efficient drainage mode and created great subglacial channels eroding into the bed, hence forming the tunnel valleys (Kehew, Piotrowski, & Jørgensen, 2012).

In the North Sea basin, three episodes of regional glaciation have been identified in the Middle and Upper Pleistocene sediments, known as the Elsterian, the Saalian and the Weichselian glaciation (Halvorsen, 2012). During this period the British-Irish and Fennoscandian ice sheets were covering large areas in the North Sea. Clark et al. (2010) presented possible scenarios regarding the breakup of this North Sea ice cover. One theory is that the lowered ice elevations due to deglaciation led to water from ice-dammed lakes to penetrate beneath the ice. This caused a collapse of the ice-bridge between Norway and Britain and formed subglacial valleys. It is also suggested that some of the North Sea tunnel valleys are the erosional record of such an event (Halvorsen, 2012).

The infill of tunnel valleys varies, but since they often occur during glaciations, it is regularly dominated by sediments from glaciofluvial sands and gravity flows, producing coarse-grained, porous and permeable material. This provides them the potential of acting as pathways with high permeability, creating transport routes as well as storage volumes for fluids, like gas. Halvorsen (2012) mapped the tunnel valley system present in the area of block 2/4, suggesting the possibility of the system acting as migration paths and hosts for the blowout gas. The interpreted outline of the tunnel valley multiple at 272 TWT (two-way travel time) can be seen in Figure 2.3.1. The branching of the valleys is clearly visible and marked with dashed lines.

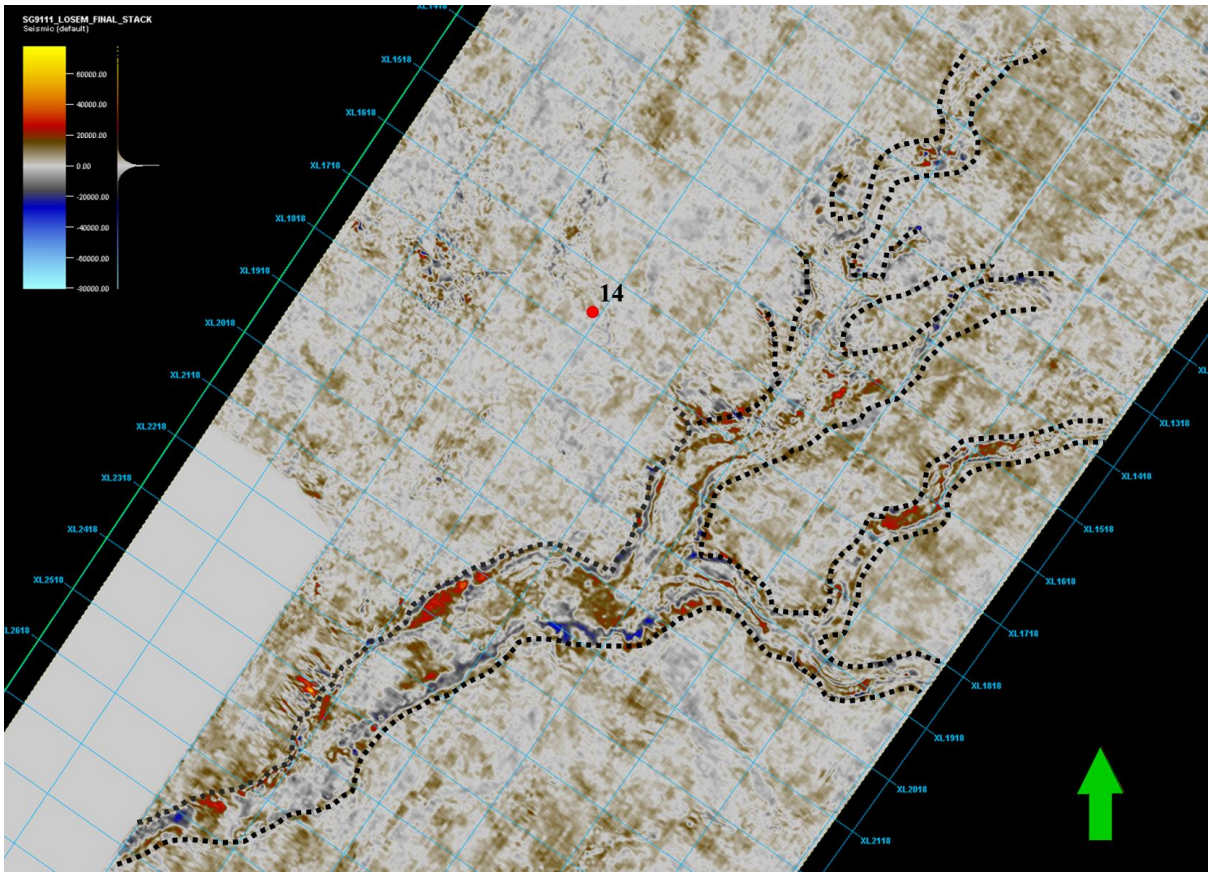

Figure 2.3.1: *Interpreted outline of the tunnel valley multiple from a time-slice at 272 ms two-way travel time. The tunnel valleys are marked with dashed lines and Well 2/4-14 is indicated with a red circle.*

3 Available data

The database that is provided for studying in this thesis is three raw seismic datasets from the SG8845_804, SG9010_804 and ST09322_8004 surveys. These seismic 2D surveys are acquired along line 804 and have been provided by Equinor.

3.1 Acquisition Setup Across Surveys

Prior to drilling the exploration well 2/4-14, a seismic site survey was acquired for Saga Petroleum the summer of 1988. After the blowout, a number of surveys of high-resolution seismic were frequently acquired, each consisting of several 2D shallow seismic reflection lines. The second dataset investigated in this thesis was acquired in May of 1990. During the acquisition in 1988, seismic repeatability was not considered, which is also the case for the first repeated lines in 1990. Still, the same parameters as the pre-drill site survey were used for data acquired in 1990, yielding relatively good repeatability. In 2009, 20 years later, Statoil acquired another site survey, repeating several of the same lines which can be seen in Figure 3.1.1. Line 804 is marked in dark blue and is the third dataset provided for this study. The line intersects with the position of Well 2/4-14 marked in the figure.

Acquiring data with a time span of 20 years provides the possibility of an extensive time-lapse seismic study on the Norwegian shelf. It may be emphasized that the seismic data was not acquired with the intention of studying the subsurface at depths as shallow as is investigated in this project.

The seismic data provided contains data for approximately 6.4, 6.8 and 9.2 km, for 1988, 1990 and 2009, respectively. The surveys were acquired with a shot point interval of 12.5 m for a total of 96 receivers. The source depth is 3 m and the water depth is 68 m. The 1988 and 1990 data are provided with geometry, and a difference in the CDP sorting was identified, which is corrected for. Seen in relation to the specialization project, the well is now located at CDP 1514. The 2009 data is provided as raw data without geometry, but with a P1/90 geometry file and observation logs containing the information required to set up a geometry assignment in ProMAX.

The repeatability of the data is adequate, and the 2009 dataset is acquired with the purpose of monitoring and comparison with earlier acquisitions. However, there are some issues addressed in the following. First, the data from 1988 and 1990 are shot in the direction from southeast to northwest, while the data from 2009 is acquired in the opposite direction. The azimuth angles for the 1988 and 1990 surveys is 305° and for the 2009 survey, it is 125°.

The near offset for the 1988 and 1990 data is 78 m. However, due to differences in the setup of the towed objects in 2009 with the streamer towed at an angle, the near offset for this data is 19.2 m with a perpendicular offset of 13.65 m. This is needed to be taken into consideration when the geometry assignment is performed. A displacement of 34 ms is also corrected for. The setup together with a table summarizing the positions of the towed objects during acquisition of the 2009 data is displayed in Figure 6.2.1. It is also noted that the 1990 data has a displacement of approximately 3 ms, probably due to repeatability issues, which is corrected for in MATLAB.

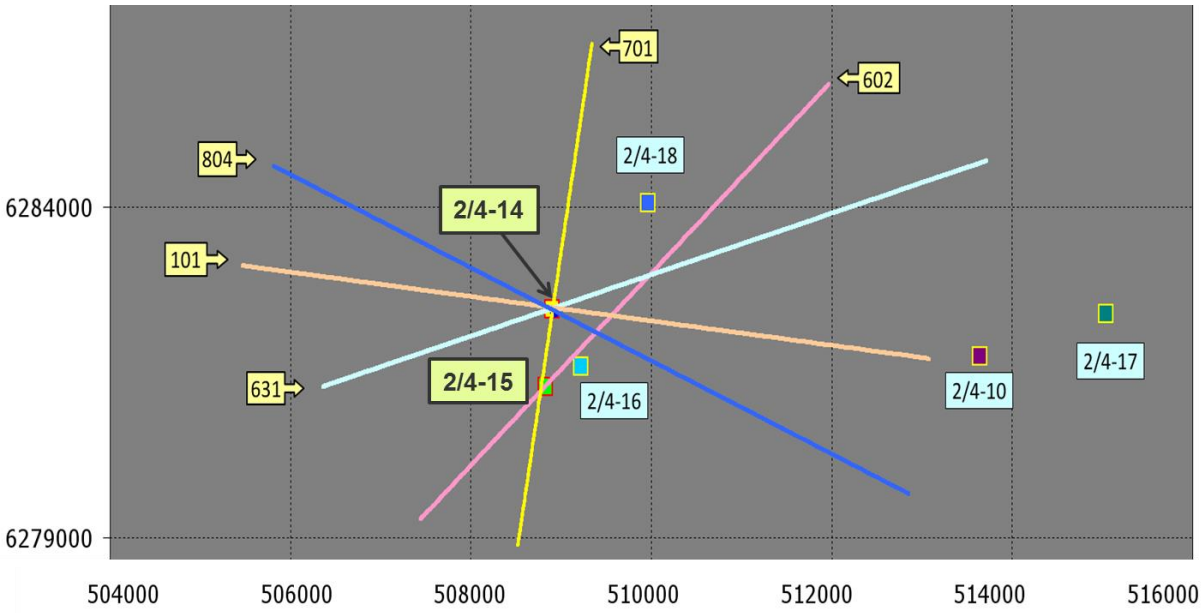

***Figure 3.1.1**: Illustration of the arrangement of the seismic lines repeated in 2009, together with the wells drilled in the area. Line 804 is marked in dark blue and intersects the blowout well (Landrø M. , 2011).*

4 Theory

This chapter presents the research done in this study within a theoretical frame. Starting by introducing the concept of 4D seismic and repeatability, followed by an introduction to time-lapse refraction seismic. The derivation of equations used in this study is also presented. The principle of reciprocity is explained, followed by a section on filtering and on the software used throughout this thesis.

4.1 4D Seismic and Repeatability

4D seismic, also known as time-lapse seismic or repeated seismic, is a phrase describing the utilization of two or more seismic surveys acquired over the same area to detect changes that have occurred over calendar time (Landrø & Amundsen, 2018). The most common practice of 4D seismic is to assess changes in a producing reservoir as well as the surroundings, such as changes in pore pressure, fluid saturation or temperature. There are many benefits with using this technique, such as increased hydrocarbon production by infill drilling and early detection of unwanted reservoir developments such as sudden pressure changes and gas breakthrough (Landrø & Amundsen, 2018). This interpretation technique also provides the ability to monitor near-surface effects, geohazards like the before and after effects of earthquakes as well as monitoring underground storage of CO_2 (Landrø & Amundsen, 2018).

4D seismic can be acquired by repeating 2D seismic lines or by repetition of larger 3D surveys. Fields can also be assessed by trenched receiver cables at the seafloor, providing a nearly continuous monitoring of the reservoir. What probably was the first 4D study performed in the North Sea was launched in 1989, due to the underground blowout in well 2/4-14 (Landrø & Amundsen, 2018).

Changes in parameters like pore pressure, temperature, fluid saturation, and thickness will occur within a producing field. These types of changes are essential to link to the seismic parameters when it comes to time-lapse analysis. In rock physics, changes in velocities to can for instance be related to fluid saturation, usually done by the aid of the Gassmann model (Landrø M. , 2010). This is a model that describes the fluid sensitivity of porous, isotropic rocks at seismic frequencies (Avseth, 2010).

The data quality in time-lapse seismic is dependent on the complexity of the geology. However, one of the greatest issues regarding the data quality is the repeatability, where the acquisition

of the seismic data needs to be repeated as accurate as possible. The repeatability can be measured in NRMS-levels. This repeatability is affected by many factors, for instance, changes in weather conditions, temperatures, tidal effects, shot-generated noise as well as noise from other vessels and differences in acquisition equipment. The most critical of these factors are however the repeatability of source and receiver positions (x, y and z coordinates), where a difference of only a few meters can have a large impact on the quality of the data and may influence the results greatly (Landrø M. , 2008).

4.2 Time-Lapse Refraction Seismic

Although the most precise results from time-lapse seismic are obtained by repeating 3D reflection data, time-lapse refraction seismic may produce details not detected with conventional reflection seismic methods (Landrø & Amundsen, 2017). Using time-lapse refraction seismic as a monitoring technique was first introduced by Landrø et al. (2004). The basic principle behind this technique is; If the hydrocarbons originally filling the reservoir are replaced with a different fluid, the velocity in the layer will change, and hence the refraction angle and travel time will change accordingly.

Reflection data from shallow seismic are usually influenced by seabed multiples and often of low resolution. Due to the data quality, the possibility of analyzing and interpreting reflectors and reflection data is limited. On the contrary, refraction seismic is not as affected by these limitations at shallow depths and may provide better opportunities for analysis within some fields of study. Shallow seismic is in this thesis referred to as seismic shallower than 500 meters.

The analysis of time-lapse seismic can be sorted in two categories. The first is based on the detection of amplitude changes, the second on detecting travel time changes. The amplitude method is demonstrated to be most robust and is the most employed method. As the accuracy of 4D seismic improves, accurate measurements of small time-shifts are also making its entry (Landrø & Amundsen, 2018).

4.3 Refractions and Time-shifts

The term refraction used within geophysics is not specific (Landrø M. , 2008). The meaning behind the concept is that a wavefront will change its direction, across an interface from one medium to another, mathematically expressed by Snell's law $\left(\sin\frac{\theta_1}{v_1} = \sin\frac{\theta_2}{v_2}\right)$, the wave is refracted. These types of waves are also referred to as headwaves, since they arrive ahead of

the direct wave at larger offsets (Landrø & Amundsen, 2017). When normally using the term time-lapse refraction, headwaves, post-critical waves as well as diving waves are exploited.

Seismic refraction methods study the waves that are refracted in which the incident and reflected angles are critical, meaning that waves that predominantly travels horizontally when compared to reflected waves are investigated. This approach can be useful when investigating increasing velocity gradients and to locate features with anomalous high velocities within areas of lower velocity (Schlumberger, 2018).

Refraction seismic is commonly performed along 2D lines where the distance between source and receiver is required to be larger than the depth of the interface that is investigated. The main difference between seismic refraction and reflection methods is the offset being larger in relation to the depth of the interface of interest. This results in the principle difference of a mainly horizontal travel paths for refractions, in contrary to the more vertical travel path of reflections. This principle is illustrated in Figure 4.3.1, showing a schematic illustration of a refracted wave passing through a two-layered model with a velocity increase across the interface. The medium is assumed to be isotropic and homogeneous.

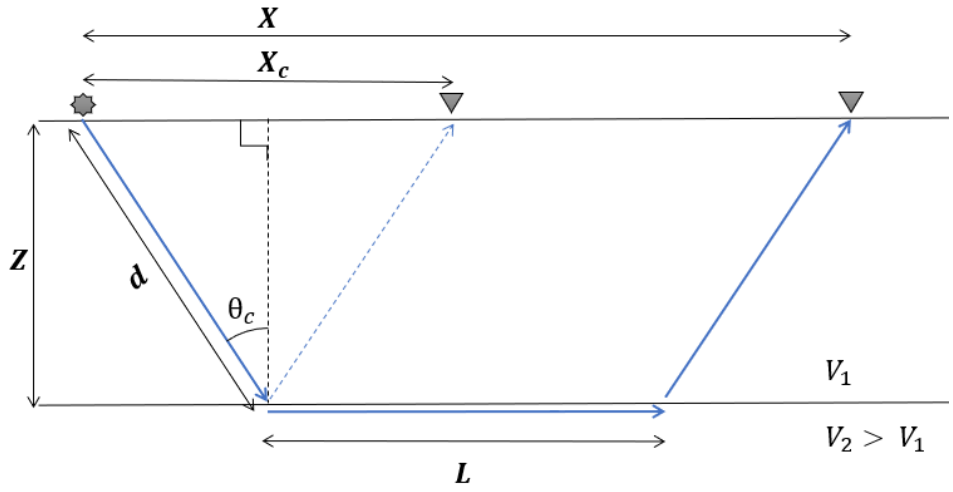

Figure 4.3.1: *A schematic illustration of the ray path of a refracted wave in a two-layered medium with an increase in velocity. The source and receiver are separated by the offset X. The interface is located at depth Z. At the critical offset X_c and at the critical angle θ_c the wave is refracted and travels the distance L through the high velocity layer. d represents the distance the wave travels in the low velocity medium.*

By assuming plane wave propagation, the travel time for the refracted wave at offsets larger than the critical offset can be derived as follows

$$t = \frac{X}{V} \rightarrow t = \frac{2d}{V_1} + \frac{L}{V_2} \tag{1}$$

Where $2d$ represents the incidence and reflected distance, L denotes the distance the refraction is propagating in the second layer. P-wave velocities for the first and second layer is expressed by V_1 and V_2, respectively. Given that the offset, X, is larger than or equal to the critical offset, X_c, the following expression for the travel time can be derived by substituting $L = X - X_c$ and utilizing trigonometric identities

$$t = \frac{2Z}{V_1 \cos\theta_c} + \frac{X - X_c}{V_2} \qquad X \geq X_c \tag{2}$$

$$t = \frac{X}{V_2} + \frac{2Z}{V_1}\left(\frac{1}{\cos\theta_c} - \frac{V_1 \tan\theta_c}{V_2}\right) \qquad X \geq X_c \tag{3}$$

θ_c denotes the critical angle for the interface at Z depth. Substitution by using Snell's law at the critical angle ($\sin\theta_c = V_1/V_2$) leads to

$$t = \frac{X}{V_2} + \frac{2Z}{V_1}\left(\frac{1 - \sin^2\theta_c}{\cos\theta_c}\right) \qquad X \geq X_c \tag{4}$$

By using the Pythagorean identities, the following expression is obtained

$$t = \frac{X}{V_2} + \frac{2Z}{V_1}\left(\frac{1 - \sin^2\theta_c}{\sqrt{1 - \sin^2\theta_c}}\right) \qquad X \geq X_c \tag{5}$$

Simplifying the expression by again applying Snell's law gives an equation for the travel time of a refraction

$$t = \frac{X}{V_2} + \frac{2Z}{V_1}\sqrt{1 - \left(\frac{V_1}{V_2}\right)^2} \qquad X \geq X_c \tag{6}$$

This equation has the linear form of $y = ax + b$, where $\frac{1}{V_2}$ represents the slope and the last term gives the intercept at the y-axis.

Changes in velocity affect the travel time. Assuming a small change in velocity within the high-velocity medium, i.e. a change in V_2 by ΔV_2, an expression for the refraction time-shift Δt can be estimated. Keeping X, Z, and V_1 constant, assuming $X > X_c$, the derivative of the expression in equation (6) gives the time-shift for the refracted event expressed as

$$\Delta t \approx -\left(X - 2Z\frac{V_1}{\sqrt{V_1^2 - V_2^2}}\right)\frac{\Delta V_2}{V_2^2} \qquad X \geq X_c \qquad (7)$$

From equation (7) it is clear that the time-shift increases linearly with offset. In the event of a 2D-anomaly, limited by the extent, E, the time-shift will be offset-dependent. Figure 4.3.2 shows a schematic illustration of this scenario. X_c' is the critical offset within the anomaly.

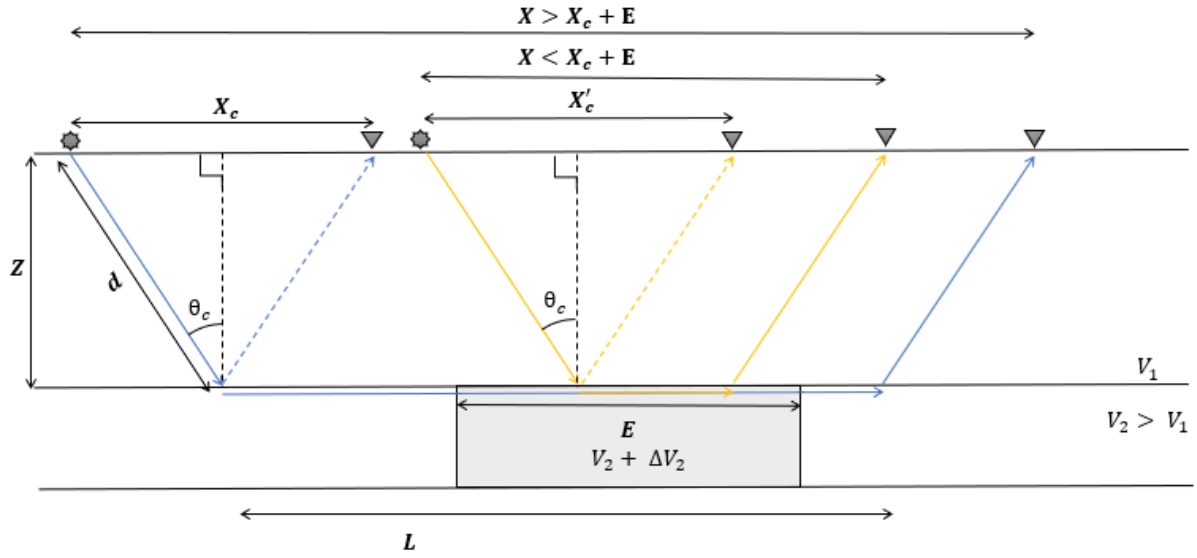

Figure 4.3.2: *A schematic illustration of an anomaly with the velocity $V_2 + \Delta V_2$ within the layer with velocity V_2, limited by the extension E. The figure is inspired by (Zadeh & Landrø, 2011).*

By following the derivation of Zadeh & Landrø (2011), as shown below, two different monitor travel time scenarios may be presented

$$t' = \sqrt{\frac{X_c^2 + 4Z^2}{V_1}} + \frac{E}{V_2'} \qquad X \geq X_c + E \qquad (8)$$

And

$$t' = \sqrt{\frac{X_c'^2 + 4Z^2}{V_1}} + \frac{X - X_c'}{V_2'} \qquad X_c < X < X_c + E \qquad (9)$$

V_2' refers to the weighted average velocity in the high velocity medium. By assuming a small change in velocity and using the first derivative of the travel time, the refraction time-shift can be estimated as follows

$$\Delta t \approx -E \frac{\Delta V_2}{V_2^2} \qquad X \geq X_c + E \qquad (10)$$

and

$$\Delta t = -\left(X - \frac{2ZV_1}{\sqrt{V_2^2 - V_1^2}}\right)\frac{\Delta V_2}{V_2^2} \qquad X_c < X < X_c + E \qquad (11)$$

The above equations (10 and 11) shows that the time-shift starts at X_c and increases linearly until reaching a maximum time-shift at offsets larger or equal $X_c + E$. For offsets smaller than X_c, the time-shift equals zero.

4.4 Diving Waves

In a zone with a gradual increase in velocity with depth, the downward component of a seismic ray may be reversed and bend the ray back towards the surface. These types of waves are commonly called diving waves as they "dive" into the subsurface and turns around without a clear reflection event (Landrø & Amundsen, 2017). A schematic illustration of a diving wave can be seen in Figure 4.4.1. As with headwaves, diving waves need large offsets in order to be detected, and although they are different wave types they are often placed in the same category. This is often convenient as it may be a challenge to discriminate between them.

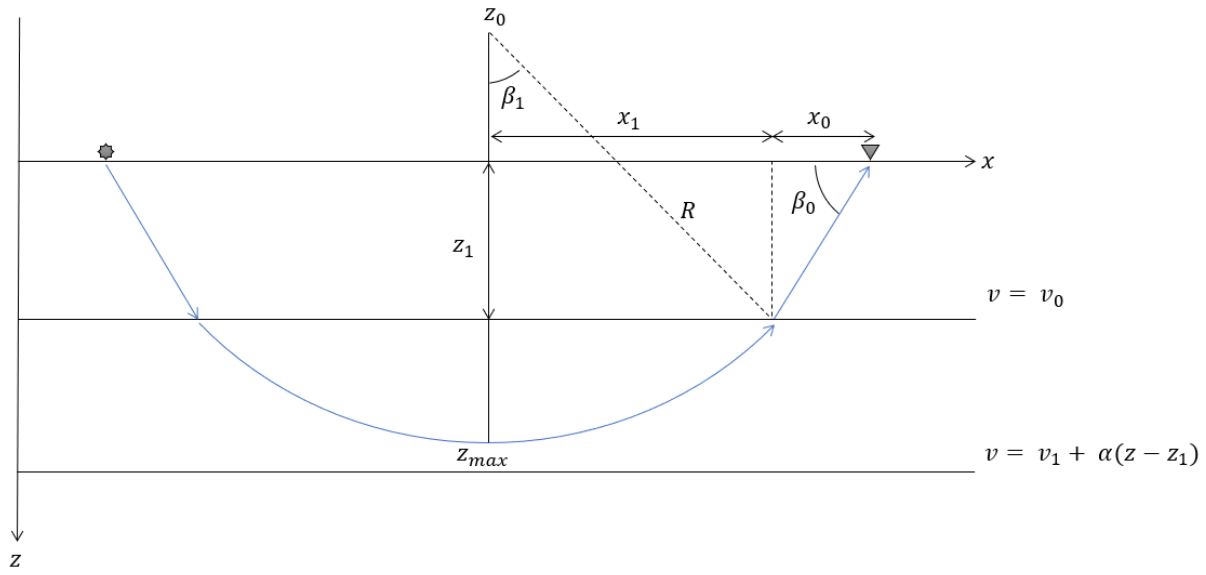

Figure 4.4.1: *A schematic illustration of a diving wave occurring in an increasing velocity medium, with the ray path occurring as an arc of a circle with radius R and centre at Z_0, where the velocity equals zero in the case of the same gradient existing everywhere. The figure is inspired by Kazei et al. (2013).*

Figure 4.4.1 shows the travel path of a ray passing through a homogeneous half-space followed by a deeper medium with a linear velocity gradient. Within the gradient domain, the wave develops into a diving wave taking the shape as an arc of a circle with its center located on the line with zero velocity. The travel time for a diving wave passing through this kind of medium can be derived as the following;

A diving wave is generated as the velocity v increases linearly with the depth z. By setting the velocity in the homogeneous half-space as $v = v_0$ and the velocity within the gradient medium as $v(z) = v_1 + \alpha(z - z_1)$, happening at the depth $z_0 = z_1 - \frac{v_1}{\alpha}$, the diving wave's ray path can be expressed as a circle with the radius R, as shown below

$$R = z_{max} - z_0 = z_{max} - z_1 + \frac{v_1}{\alpha} \tag{16}$$

Letting X be the offset and T the travel time for the ray connecting the source and receiver as shown in the following equations

$$X = 2(X_0 + X_1) \tag{17}$$

$$T = 2(T_0 + T_1) \tag{18}$$

T_0 represents the time the ray spends in the constant velocity medium as a straight line, and T_1 is the time spent by the ray on the circle between the interface and the largest depth. With z_0 as defined above and by using the geometric relation $z_1 - z_0 = R\cos\beta_1$ this leads to the expression

$$R\cos\beta_1 = \frac{v_1}{\alpha} \tag{19}$$

By using Snell's law $\left(\frac{\cos\beta_0}{v_0} = \frac{\cos\beta_1}{v_1}\right)$ this leads to the expression

$$\cos\beta_0 = \frac{v_0}{\alpha R} \tag{20}$$

Then, by using trigonometric identities one can get the relation

$$X_0 = z_1\frac{\cos\beta_0}{\sin\beta_0} = z_1\frac{\frac{v_0}{\alpha R}}{\sqrt{1-\left(\frac{v_0}{\alpha R}\right)^2}} = \frac{z_1}{\sqrt{\left(\frac{\alpha R}{v_0}\right)^2 - 1}} \tag{21}$$

Finally, in the constant velocity layer, the travel time can be expressed as

$$T_0 = \frac{z_1}{v_0\cos\beta_0} = \frac{z_1}{v_0\sqrt{1-\left(\frac{v_0}{\alpha R}\right)^2}} \tag{22}$$

By using both the geometric relation

$$x_1 = R\sin\beta_1 \tag{23}$$

Together with equation (19), this provides

$$x_1 = \sqrt{R^2 - \left(\frac{v_1}{\alpha}\right)^2} \tag{24}$$

Integration over the circle's arc yields the following expression for T_1

$$T_1 = \int_0^{\beta_1} \frac{R}{v(\beta)} d\beta \; = \frac{1}{\alpha} \operatorname{arccosh}\left(\frac{\alpha R}{v_1}\right) \tag{25}$$

Finally, by using equations (17) and (18) we obtain the expressions for offset X and two-way traveltime T of the ray

$$X = \frac{2z_1}{\sqrt{\left(\frac{\alpha R}{v_0}\right)^2 - 1}} + 2\frac{v_1}{\alpha}\sqrt{\left(\frac{\alpha R}{v_1}\right)^2 - 1} \tag{26}$$

And

$$T = \frac{2z_1 \alpha R}{v_0^2 \sqrt{\left(\frac{v_0}{\alpha R}\right)^2 - 1}} + \frac{2}{\alpha} arccosh\left(\frac{\alpha R}{v_1}\right) \tag{27}$$

The higher the velocity gradient, the earlier the ray prefers to turn around, hence the observed offset will also be shorter. By comparing the travel times for refracted waves or headwaves with the travel time for diving waves, shows that for shorter offsets these are nearly identical and almost impossible to distinguish between, at low frequencies (Landrø & Amundsen, 2017).

4.5 The Principle of Seismic Reciprocity

The reciprocity principle implies that the time required for seismic energy to travel from the source to receiver is the same, independent of the direction. Hence, the travel time will not change even though the positions of source and receiver are interchanged. This is an important concept in seismic and relations regarding reciprocity are found in many disciplines of physics (Knopoff & Gangi, 1959). For instance, this is applied in depth calculations and quality control checks in the field (Geometrics, 2018). When applying this principle, the same seismogram should be recorded, and a physical reason for the validity of this principle is that the speed of sound along the ray is the same in either direction, regardless of geometrical arrangement and complexity within the earth (Claerbout, 2010).

In this study a time-lapse refraction assessment is carried out, using three seismic surveys. Repeatability is an important factor and since the third dataset is acquired in the opposite direction, the principle of reciprocity applies in this case. By assuming it to be valid, source and

receiver may be interchanged and still yield the desired results for travel times. However, the principle may not be valid for amplitude studies due to directivity effects, which will be dependent on shooting direction. During the specialization project, the time-shift analysis was performed in the shot-domain, due to the acquisition directions being different, this is not possible unless the principle of reciprocity is valid, and the source and receivers can be interchanged. Another solution is to sort and match all three datasets in the CDP-domain so that the time-shift analysis will not be dependent on acquisition direction.

4.6 Filtering

Noise may be present in a dataset for many reasons. In order to remove the unwanted noise, different types of filters can be applied. A filter is defined as a linear transformation of an input time series into an output time series. It is assumed that the filter is time-invariant and linear (Arntsen, 2015). Some of the most common filters are the low-pass filter, which removes high-frequency noise, and the high-pass filter, which eliminates low-frequency noise (i.e. swell noise) and is often used pre-stack to suppress acquisition noise. The most common form of filtering is to apply a bandpass-filter, which does both and can be designed to attenuate noise and remove unwanted frequency components (Arntsen, 2015).

4.7 Software

Throughout this project, the three datasets have been processed by using the software ProMAX and MATLAB. These are academic licenses and intended for students at NTNU.

The ProMAX SeisSpace software is a commercial seismic processing system and is developed by Landmark Solutions. The program is intended for 2D or 3D pre- and post-stack surveys of large volumes, both for land and marine surveys. The system is comprehensive and combines parallel processing, geophysical algorithms, and analysis tools in order to distribute large volumes of processed data. The software was in this thesis used to process the given seismic raw data in several flow steps (Halliburton Landmark, 2017).

The analysis of the seismic data and time-shift results was done in MATLAB (matrix laboratory). MATLAB is a programming platform developed by MathWorks. The language is matrix-based and integrates programming and visualization computation into an interactive environment. The software is optimized to solve scientific and engineering problems (MathWorks, 2017). During this project, MATLAB was primarily used for analyzing, calculating parameters and constructing plots.

5 Methodology

The aim of this thesis is to perform a time-lapse refraction analysis on three 2D seismic surveys, acquired along line 804 within a time span of 20 years, to monitor a shallow gas migration. The basic principle is to utilize the horizontal energy obtained by refraction seismic to detect variations in velocity at shallow depths, where the contribution from conventional reflection methods may be limited. The analysis is performed through several steps, which will be addressed in this section. As previously mentioned, this is a continuation of preceding research performed only on the 1988 and 1990 data. The addition of the third dataset from 2009, includes changes in the geometry due to opposite acquisition direction and different acquisition parameters. In order to perform the study consistently, all three datasets have to be reprocessed. The method of cross-correlating the data needs adjustments to be executed in the CDP-domain rather than the shot-domain.

The main part of the processing is performed in ProMAX. The first step is to set up and match the geometry of the three datasets. Limited processing is applied to the data. However, a bandpass-filter is applied. The 2009 data is provided as raw data together with a P1/90-file and observation logs containing the necessary information to perform a geometry assignment. The geometry is set up, and it is ensured that the data matches on the closest CDP location. Seen in relation to the specialization project, the location of well 2/4-14 is changed to CDP 1514.

In the shot-gather, the refractions are identified, and specific events can be chosen. Two refractions for different depths are investigated. First, a refraction tracked for larger offsets, approximately 728 m to 1253 m is considered. Then another refraction for shorter offsets tracked from approximately 478 m to 853 m. The two refractions are initially studied separately. After identifying refractions, the data is alternated, and a standard windowed cross-correlation is performed. This process involves picking time-gates and designing the time-window. Then the cross-correlation is executed within a chosen offset range. This function requires the length of the window, the top of the window, the offset range and the allowed time-shift. The cross-correlation procedure involves some testing and is essentially the core of the results. This process is executed in three turns.

1) The baseline is pre-drill (1988) and the monitor is post-blowout (1990), thus wanting to detect anomalies within this time span.

2) The 1990 data acts as baseline and the 2009 data is monitor, producing time-shifts from approximately a year after the blowout and 20 years later.
3) The 1988 and 2009 data are cross-correlated, enabling time-shifts from before and 20 years after the blowout to be detected.

The time-shift values for each chosen offset are exported into MATLAB for further processing, plotting, and analysis. The values including the 1990 data are corrected for a 3 ms displacement. The time-shift data is smoothed using a five-point moving average function.

In ProMAX brute stacks, in addition to difference sections, for all three datasets are produced. This is done by a simple processing sequence involving a velocity analysis, normal moveout correction, and stacking. To be able to compare the stacks, proper scaling is also necessary. From these stacks, interpretations of tunnel valleys and changes in the subsurface through time are made.

Finally, estimations of depths of the detected anomalies are calculated. The time-shift results are combined with the stack and the interpretations of what has happened over time can be carried out.

6 Results

This chapter presents the main results from the analysis of the three seismic surveys along line 804. Starting with an overview of the general processing and the geometry setup. This is followed by the results from the produced stacks and difference sections, as well as the cross-correlated time-shifts. The time-shifts for each dataset, chosen at specific offsets are compared both with trace-plots and stacks. The results indicate gas anomalies at shallow depths, which are discussed in the next chapter.

6.1 Overview and General Processing

The goal is to process the datasets in such a matter that anomalies can be detected by changes in time-shifts for the interpreted refractions through time. The seismic surveys from 1988 and 1990 are already matched in geometry, CDP and offset location. The travel times for base and monitor data are compared by sorting the data in CDP and offset, followed by alternating the traces in pairs. The data for 1988 and 1990 are loaded into ProMAX and combined, and an overview of the alternated data can be seen in Figure 6.1.1. The trace corresponding to the baseline is the left part of the trace pair, while the trace corresponding to the monitor is to the right. The figure below shows data for CDP number 1103 and for all offsets on the x-axis, while the y-axis denotes the travel time in ms. The direct wave, reflections, and refractions are observed in the gather. Some sort of noise is noticed in the upper right part of the figure.

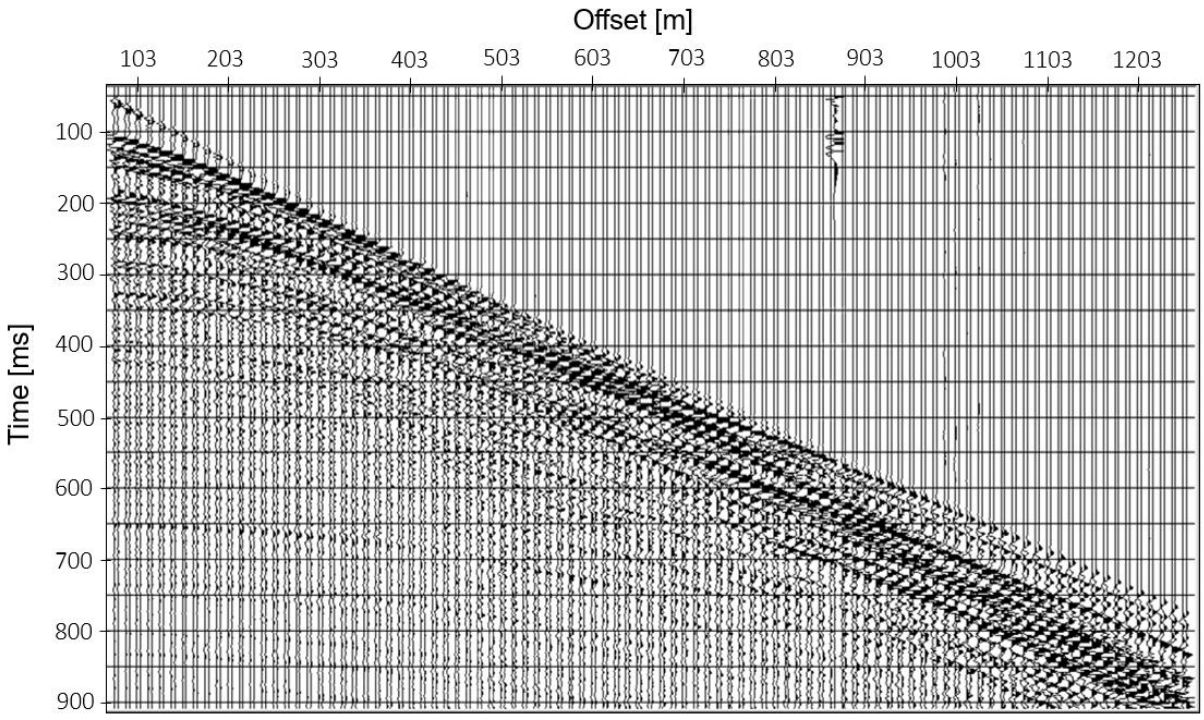

Figure 6.1.1: *Overview of the seismic data. The shot-gather contains an alternation of traces from the 1988 and 1990 surveys. CDP 1103 is displayed and the x-axis represents offset in meters, while the y-axis denotes time in ms.*

To get a better overview of the acquisition of the three surveys across line 804, the coordinates for source positions during acquisition are plotted as displayed in Figure 6.1.2. The coordinates for shot-positions from the 1988 data are marked in red, the 1990 data are marked in blue while the 2009 data are indicated in green. The location of Well 2/4-14 and the lateral extent of the anomalies observed in the time-shift results for Refraction 2 are marked with black arrows. As seen in the figure, the following can be noticed:

- Coordinates from 1990 appear to be positioned slightly more in northeast direction than the two other surveys.
- The coordinates for 1988 and 2009 have a good correlation.
- The 1990 and 2009 coordinates follow a relatively straight line, however, 2009 appears a little more deviant.

In Figure 6.1.3 a closeup of the 1988 and 1990 data is presented and illustrates the difference in positions as well as it becomes clearer that the 1990 data occurs in a straight line in contrast to the 1988 data. The approximated absolute values of the difference between shot positions for 1988 and 1990 data are illustrated on the right-hand side.

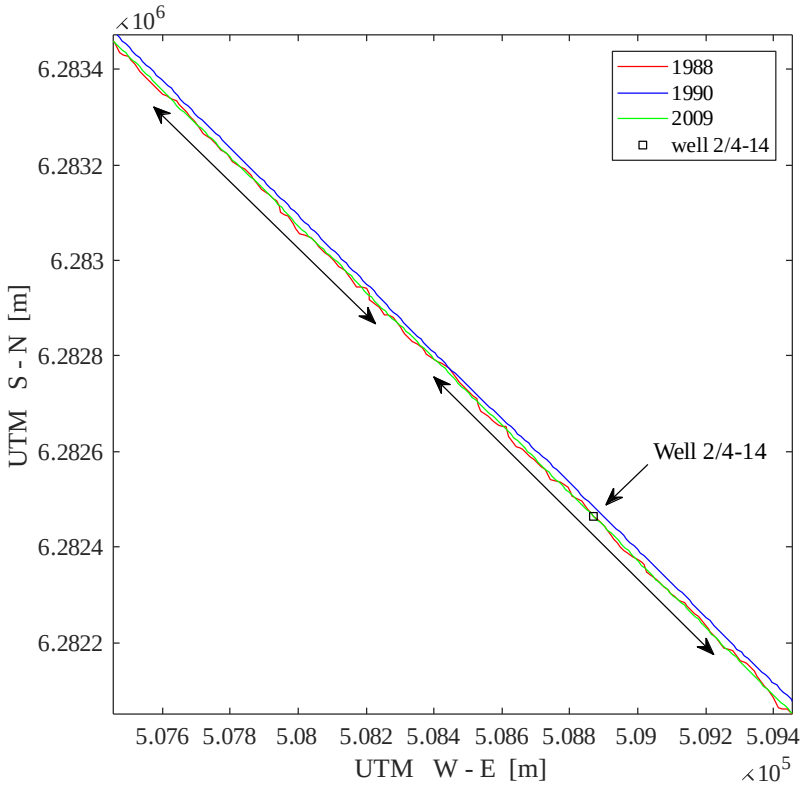

Figure 6.1.2: *Geometry acquisition for 1988, 1990 and 2009 surveys, presenting source positions. The location of the blowout well is marked with a black square.*

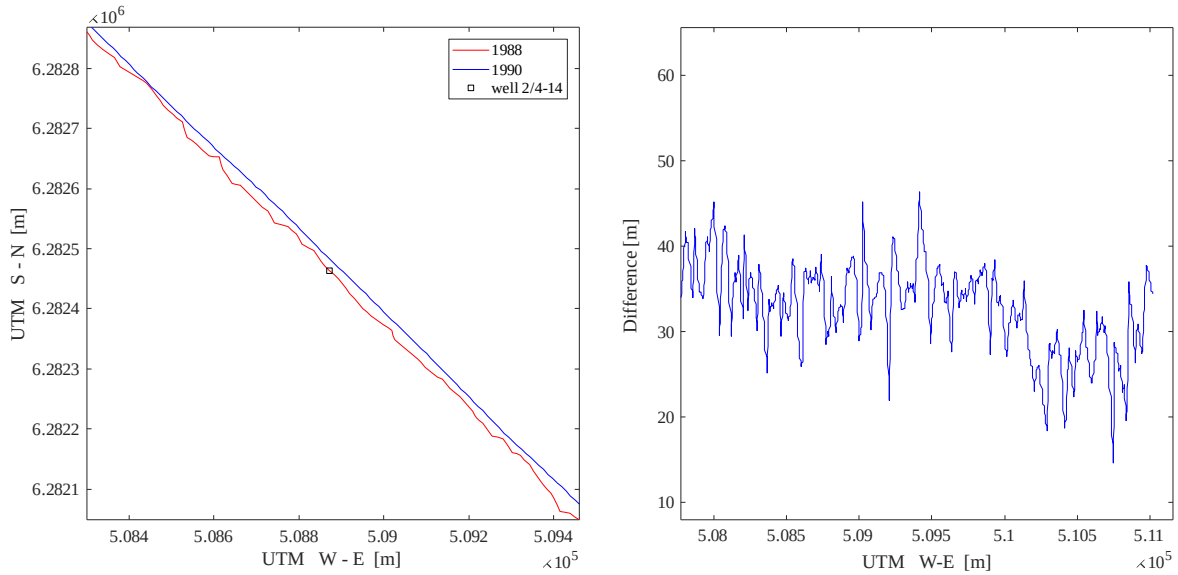

Figure 6.1.3: *To the left, a closeup of shot-positions for 1988 (red) and 1990 (blue) surveys across line 804. On the right-hand side, approximated absolute values for the difference between the 1988 and 1990 source coordinates.*

The direct wave is the wave that travels in the water layer, directly from source to receiver and is neither reflected or refracted by the subsurface layers (Landrø M. , 2008). In theory the direct wave should be similar for all three datasets, however, a displacement in the 1990-data is observed creating a pull-up effect of nearly 3 ms, indicating a shift of 3 ms for the whole dataset. This shift is probably due to some sort of repeatability issue and is corrected for in MATLAB. It is not considered to be what is in this paper referred to as an anomalous time-shift. Figure 6.1.4 shows an alternation of traces in the 1988 and 1990 data. The left side of the figure shows the direct wave, while a more detailed image illustrating the shift of 3 ms is shown to the right.

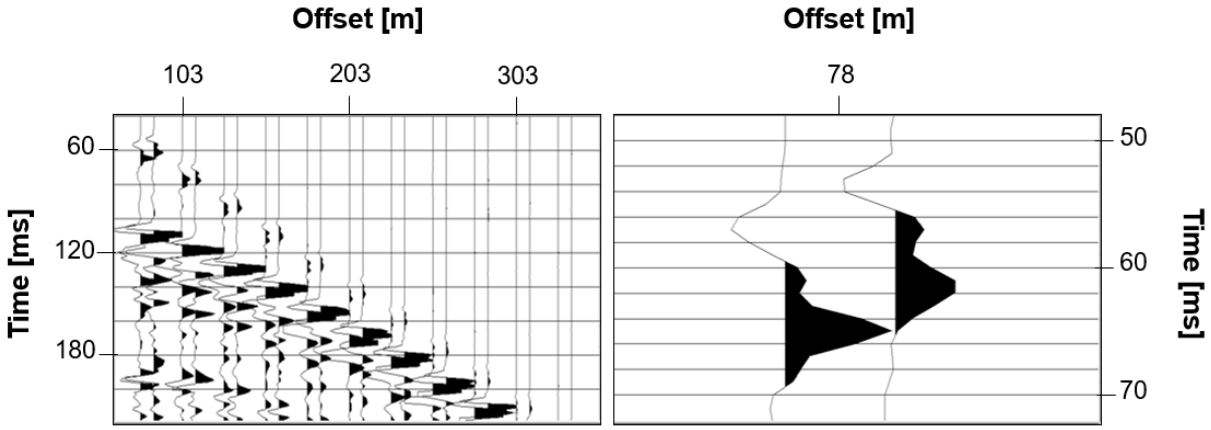

Figure 6.1.4: *Alternation of trace pairs from the 1988 and 1990 surveys. The left part demonstrates the direct wave for the first shot, where the x-axis denotes offset in meters from 78 to 341 m. A more detailed example at offset 78 m is shown to the right. A shift of nearly 3 ms is visible.*

6.2 Geometry Setup

The seismic survey acquired in 2009 is provided as raw data without geometry. However, a P1/90-file and the observation logs are given, containing information to perform a geometry assignment. This process relates the data to a description of the field geometry used during the data collection process. The geometry assignment procedure assigns each trace to a single shot and receiver, CDP, inline and crossline as well as offset bin. Other individual values for each trace, CDP, shot and offset bin are also computed (Halliburton Landmark, 2018).

As more information concerning the acquisition of the data is made available, this process is performed several times. For instance, it was discovered that the 2009 data was acquired in the opposite direction than the data from 1988 and 1990. Where the 1988 and 1990 data have a sail line azimuth of 305°, 2009 data had a sail line azimuth of 125°, hence an acquisition direction from northwest to southeast. It is also informed that the gun array and streamer are towed at an angle relative to each other. This needed to be taken into consideration when setting up the geometry.

Table 6-1 summarizes the towed objects and their positions as illustrated in Figure 6.2.1. When matching the geometry of the 2009 data with the data from 1988 and 1990, it is noticed that while the near offset is 78 meters for the two first datasets, this is not the case for the 2009 data. A different distance between source and receiver is observed. The near offset for the seismic survey from 2009 is a lot shorter than expected and is calculated to be 19.2 m with a perpendicular offset of 13.65 m. A correction of 34 ms is also done, by using the hand statics function in ProMAX.

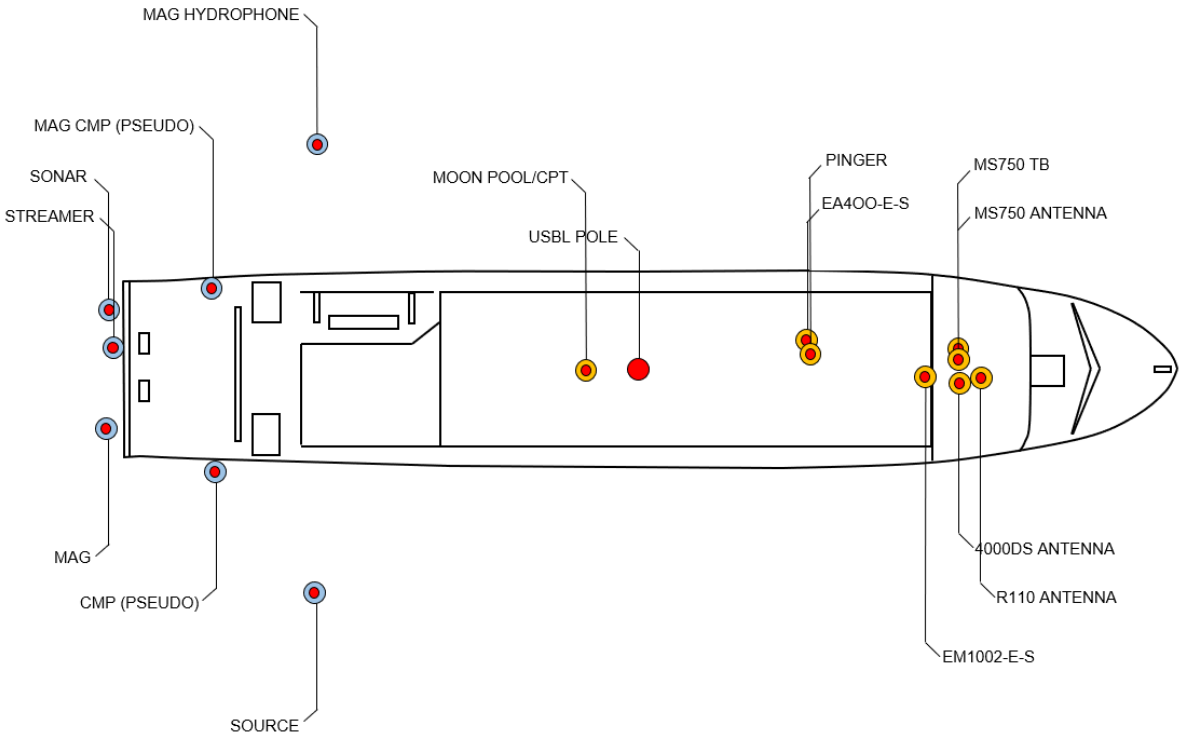

Figure 6.2.1: *Illustration depicting the different towed objects during acquisition of the 2009 data. The figure is modified from the acquisition report.*

Table 6-1: *Positions of the towed objects during acquisition of the 2009 data. The table is modified from the acquisition report.*

Towed objects (laid back positions)							
Name	x	y	z	Name	x	y	z
Sonar	-3.33	-29.30	0.00	Gun array	12.54	-68.80	0.00
CMP	5.72	-78.40	0.00	Streamer	-1.11	-88.88	0.00
Tailbuoy	0.00	-1271.15	0.00	Mag	3.33	-66.30	0.00
Mag CMP	-4.61	-72.05	0.00	Mini airgun hydrophone	-12.54	-77.80	0.00

Throughout the specialization project in 2017, the data were processed in the shot domain, sorted in FFID and recording channels. As the third dataset from 2009 was acquired in the opposite direction, the data could no longer be sorted in the shot domain. In order to be able to compare and correlate the data, all three datasets are reprocessed and sorted in the CDP domain.

6.3 Filtering

The seismic survey from 2009 reveals to be quite noisy and is influenced by low-frequency swell noise, as can be seen in Figure 6.3.1. A bandpass-filter with frequency values of 8-20-80-110 is applied in order to reduce the noise and hence improve the data. An image of the 2009 data before and after the application of the bandpass-filter is shown in the figure below. The figure displays a shot gather for CDP 1103, from channel 1 to 95 on the x-axis and travel time in ms on the y-axis. A clear improvement of the data is observed.

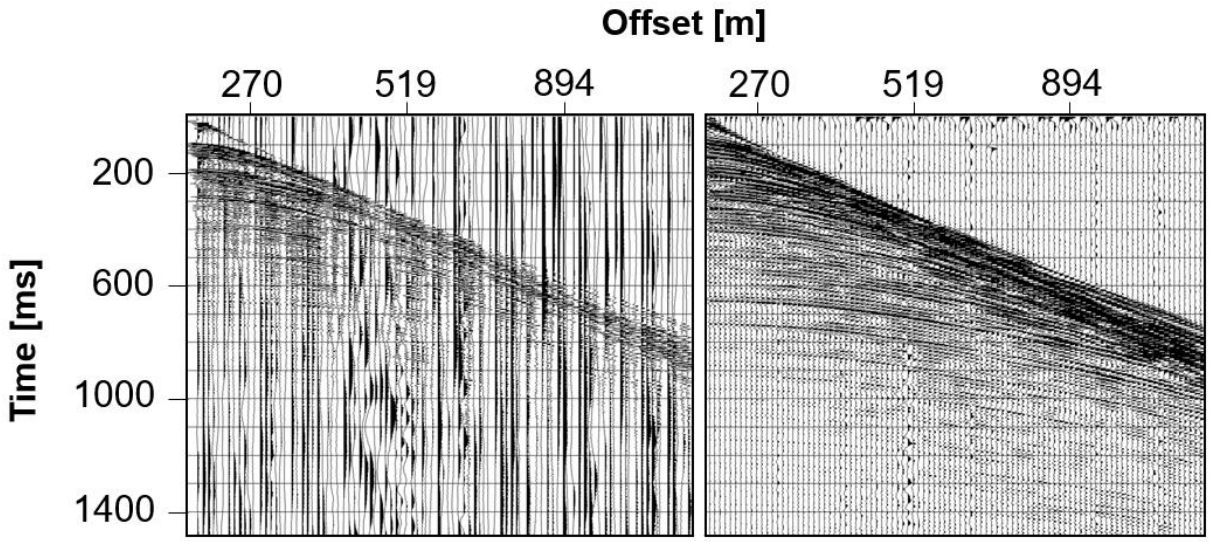

Figure 6.3.1: *2009 data before and after applying a bandpass-filter. CDP 1103 for channels 1 to 95 is displayed in both images.*

6.4 4D Time-shift Cross-correlation

The three datasets are now combined for analysis. Throughout this project, several refractions are tested and investigated. However, mainly two events interpreted as refractions are selected and indicated with red lines in Figure 6.4.1. One refraction for larger offsets, here referred to as Refraction 1, is tracked from approximately 728 m to 1253 m. The other refraction was tracked to as short as possible, from approximately 478 m to 853 m, and is referred to as Refraction 2. The figure shows the alternation of the traces from the 1988-data and 1990 data, at a CDP location far from the well in the southeast direction. The effect of the gas generating anomalous time-shifts is assumed to be absent at this location.

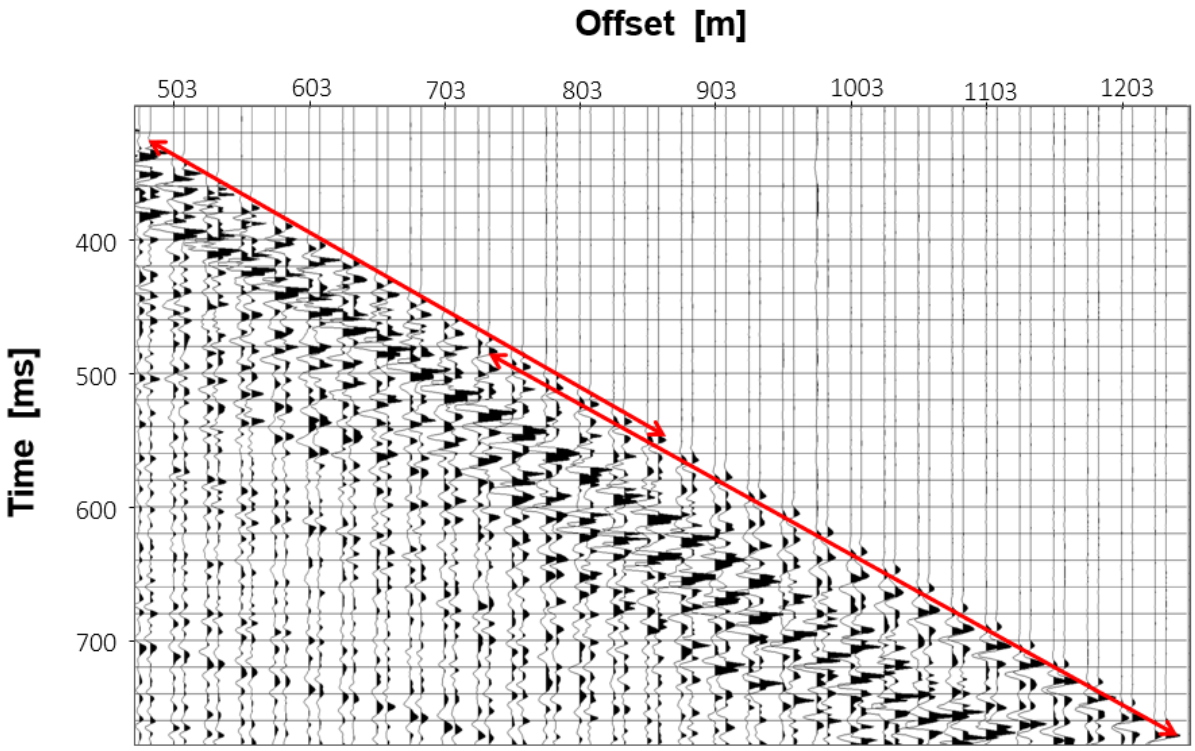

Figure 6.4.1: *Alternated traces from the seismic survey acquired in 1988 and 1990. The chosen refractions for this thesis are marked with red arrows. The x-axis denotes offset in meters and the y-axis represents travel time in ms.*

The time-shift values are produced by performing a cross-correlation technique on the data, executed in ProMAX. First, a time-gate is manually picked in the CDP gather with alternated traces for the base and monitor data. This process is tested and performed several times in order to get the results as accurate as possible. Setting a too small time-window results in cutting the signal, a too large time-window may result in signals from other reflections and refractions to infiltrate and overlap the time-shift values. The same time-gate is used for the same refraction for all the datasets. For the main results in this thesis, the length of the input traces for cross-correlation is set to 30 and 19 ms for Refraction 1 and 2, respectively.

In ProMAX, the cross-correlation function computes a correlation of input pairs of traces. The correlated output data includes the trace headers CCP_AMPL and CCP_TIME, which refers to the cross-correlation amplitude and cross-correlation peak lag time, with respect to the output trace center (Halliburton Landmark, 2018). The correlation start time is obtained from the database and is the handpicked miscellaneous time-gate. It should be noted that only the top-gate is picked. For each of the selected refractions, the output cross-correlation length parameter is specified to determine the bottom of the time-gate. The time-shifts are estimated by using a

30 ms and 19 ms time-window for Refraction 1 and 2, respectively. An example of cross-correlated data is shown in Figure 6.4.2. The figure shows the cross-correlation of the 1988 and 1990 data with results for offset 540 meters corresponding to Refraction 2, displaying an image of the CCP_TIME in the upper part. As explained in previous sections, the trend is centered at 3 ms, due to the shift detected in the 1990 data. This is however corrected for in MATLAB, resulting in the non-anomalous time-shifts to center around zero. Anomalies are clearly visible intersecting the well and in NW direction of it. The discrepancy observed in the southeast direction is considered to be some sort of noise rather than an anomaly.

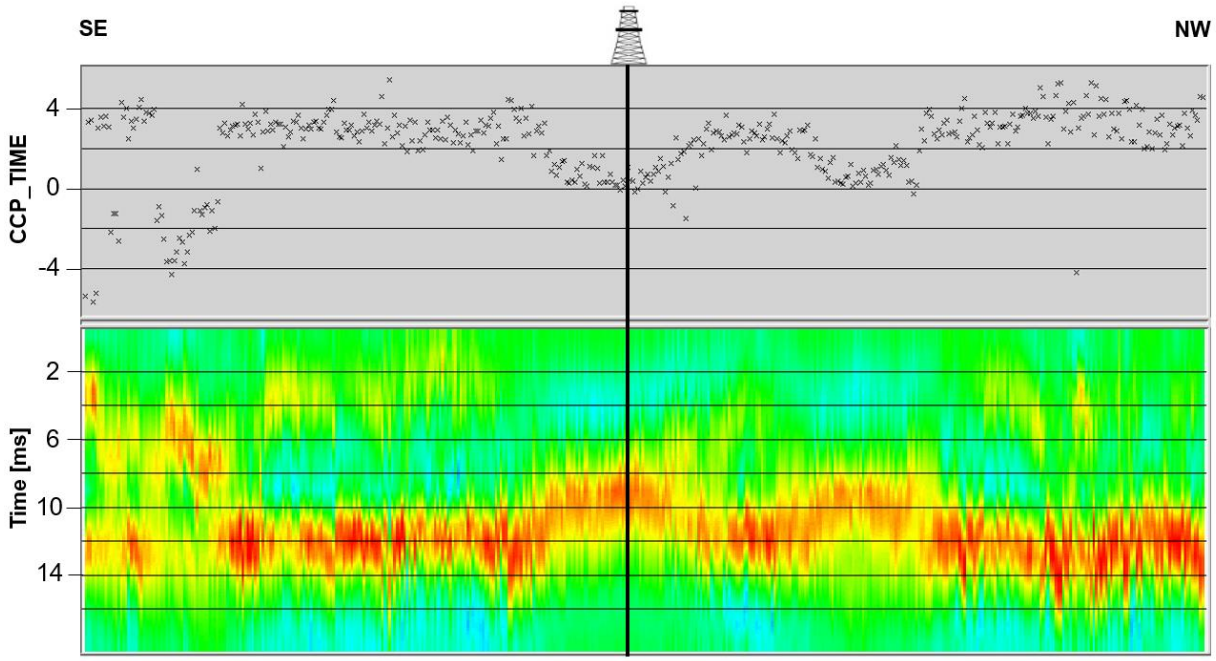

Figure 6.4.2: *An example of the cross-correlated result at offset 540 m, for 1988 and 1990 data. Anomalies can be observed in the middle of the figure. Orientation is from southeast to northwest and the well is located approximately in the middle of the figure.*

The computed CCP_TIME values, also referred to as time-shift values, for selected offsets are then transferred to MATLAB for continued processing and analysis. The results for the two chosen refractions are shown in the sections below.

6.5 Reflection Data and Stacks

Simple raw stacks, as well as stack differences, are also produced from the three datasets. A general processing sequence including NMO-correction and stacking resulted in the brute stacks shown in Figure 6.5.1. Minimal processing is applied to create the stacks, and no multiple removal or migration algorithms are performed. Despite these limitations, an analysis showing clear results is possible. The three datasets are scaled by using an automatic gain control function in ProMAX so that the stacks can be compared and interpreted in relation to each other. This gives a good overview of the situation and is beneficial to compare with, in the search for anomalies. A conventional difference section is also obtained. The figure below shows the seismic reflection data from before and after the blowout, with the difference section to the right. Tunnel valleys are clearly visible within the upper 200 ms of the stacks, in the northwest direction of the well. A brightening of reflectors is observed in the stack from 1990 when comparing it with the one from 1988, as for example at 520 ms. The difference stack is also made and shows the development through time from before and after the blowout. The difference stack highlights this brightening and shows a focus near the well. A stack of the 2009 data can be seen in Appendix A.

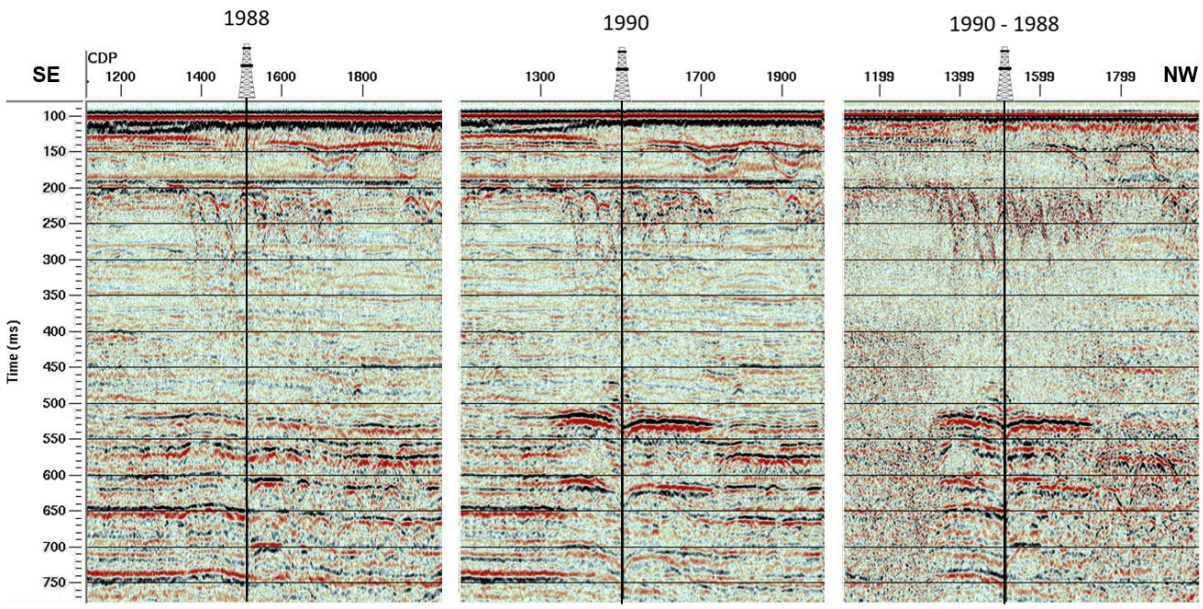

Figure 6.5.1: *Brute stacks for the 1988 and 1990 data, with a stack showing the difference section to the right.*

As this study concentrates on the shallower parts of the subsurface, close-ups of the stacks are presented in Figure 6.5.2, which displays the upper 190 ms of the data. The lower part of the figure is again a difference stack from before and after the blowout. Indications of tunnel valleys can be seen towards northwest in the figure. The tunnel valley intersecting the well is more difficult to distinguish in the stacks, however it might be more visible in the 2009 stack. The difference stack shows some brightening of amplitudes at the edges of the tunnel valleys. An interpretation of the tunnel valleys is shown in Figure 6.5.3, where the top of the layer is marked in yellow, while the tunnel valleys are highlighted in blue. Only the upper 195 ms are displayed. Difference stacks for the 2009 – 1990 data can be seen in Appendix A.

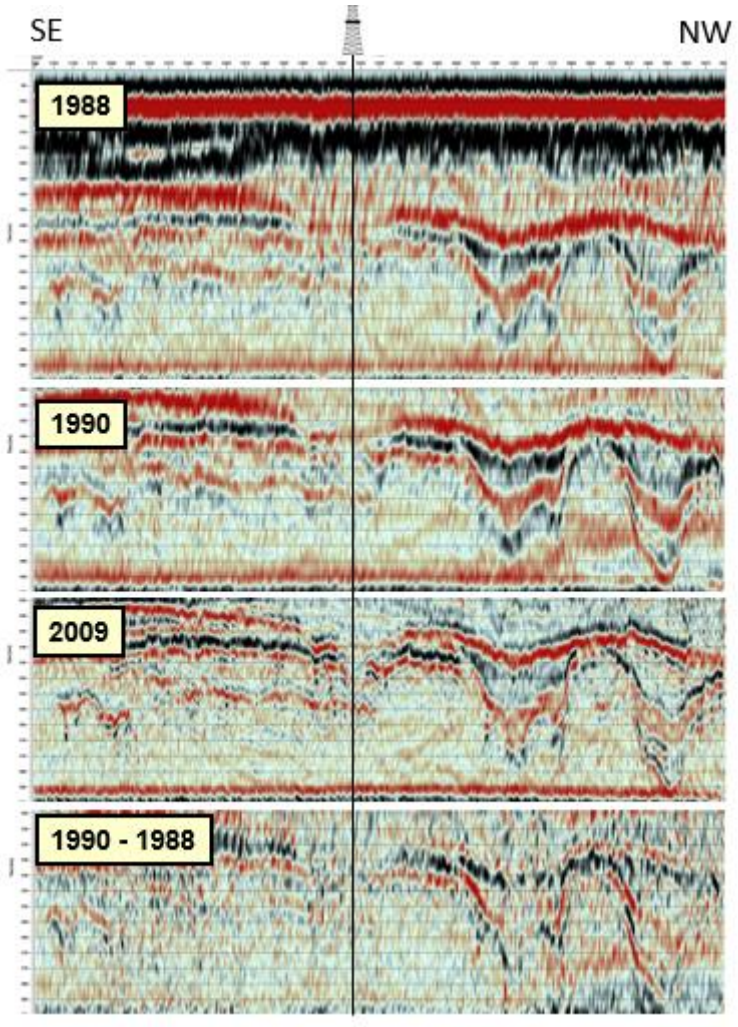

Figure 6.5.2: *Stacks from all three datasets, as well as a difference stack. Only the shallower parts (upper 190 ms) of the subsurface are displayed.*

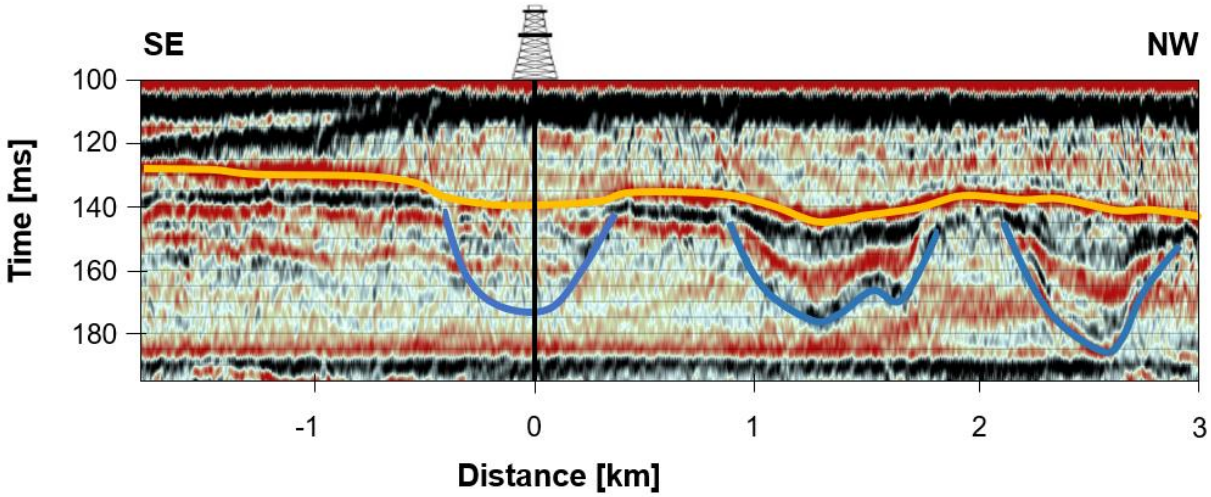

Figure 6.5.3: *Interpretation of the tunnel valley system for the upper 195 ms of the stack produced by 1988 data. The tunnel valleys are highlighted in blue, while the top of the layer is marked in yellow.*

6.6 Time-shift Results for Refraction 1

If there are no indications of an anomaly, the amplitudes will appear equal in time. When indications of an anomaly are present, amplitudes for monitor data will decrease or increase in time relative to the baseline creating a pull-up or pull-down effect. However, in the case of analysis regarding the 1990 data, a shift of approximately 3 ms needs to be taken into consideration.

The alternating traces with 1988 data as baseline and 1990 as monitor, for offsets 1140 m to 1191 m, can be seen in Figure 6.6.1. To the left traces located approximately 1 km in a southeast direction from the well is presented. This is relatively far away from the blowout well. The right part of the figure is presented with the same offset, but the traces are located approximately 200 m northwest of the well. A pull-down is noticed, yielding a time-shift of nearly 5 ms.

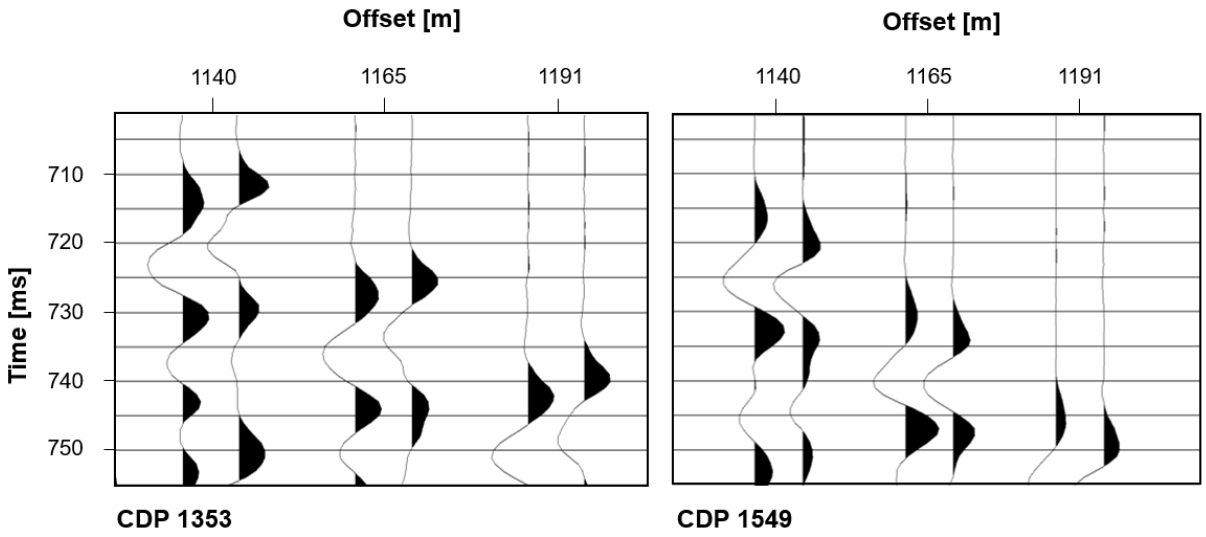

***Figure 6.6.1**: Refraction time-shift in alternated trace pairs from 1988 (base) and 1990 (monitor). On the left-hand side, CDP location far from the well in SE direction is demonstrated. On the right-hand side, CDP location close to the blowout well is displayed. The y-axis denotes travel time in ms and is the same in both figures.*

The time-shift results from the cross-correlation for the 1988 and 1990 data at offset 1191 m is presented in Figure 6.6.2. The same time-gate, time-window and offset is used for all the figures below in this section. A significant anomaly is observed, with an increase in travel time from before to after the blowout and intersecting the well which is marked with a black line. The lateral extent of the anomaly is nearly 1.5 km and there is a consistent increase in time-shift with a maximum peak of 5.7 ms 288 m NW of the well.

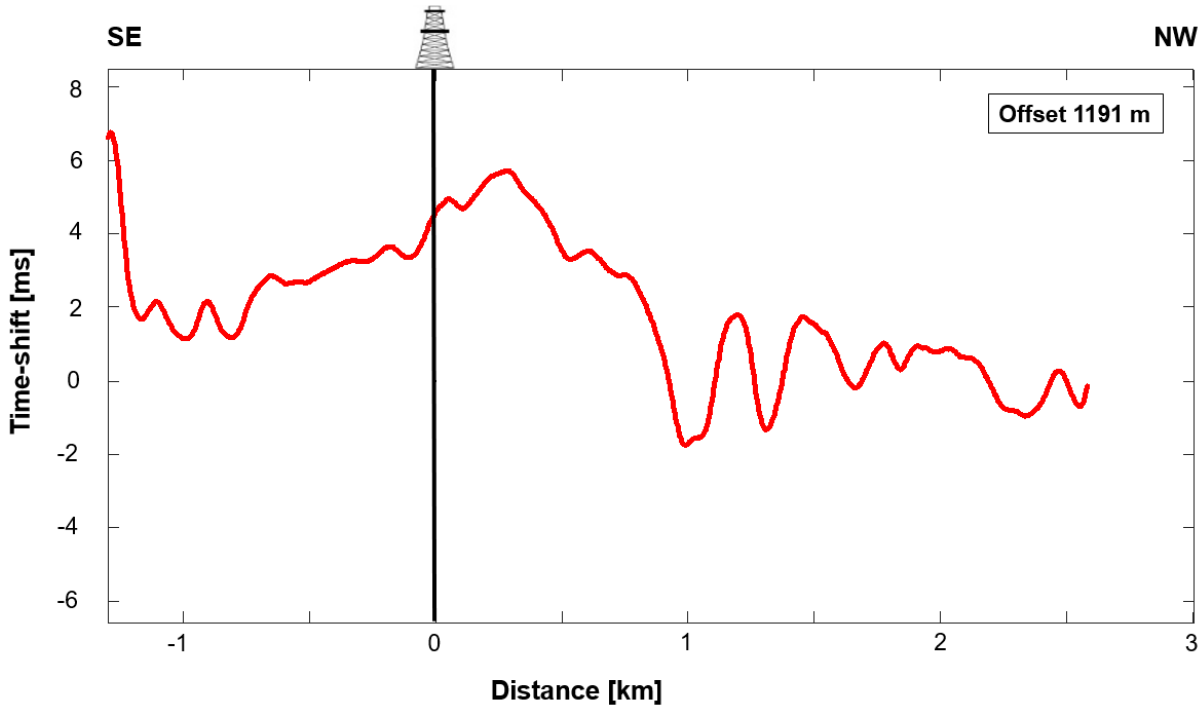

***Figure 6.6.2**: Time-shift results in ms for the cross-correlation between 1988 and 1990 at offset 1191 m, in relation to the blowout well.*

The alteration of trace pairs with the 1990 data as base and 2009 as monitor is displayed in Figure 6.6.3. To the left, locations far from the well show no significant time-shifts. As the 1990 data now acts as baseline, 3 ms pull-down is observed. To the right, closer to the well, the traces are nearly aligned in time. Taking into account the 3 ms displacement, this yields a pull-up effect with an observed time-shift of close to -4 ms.

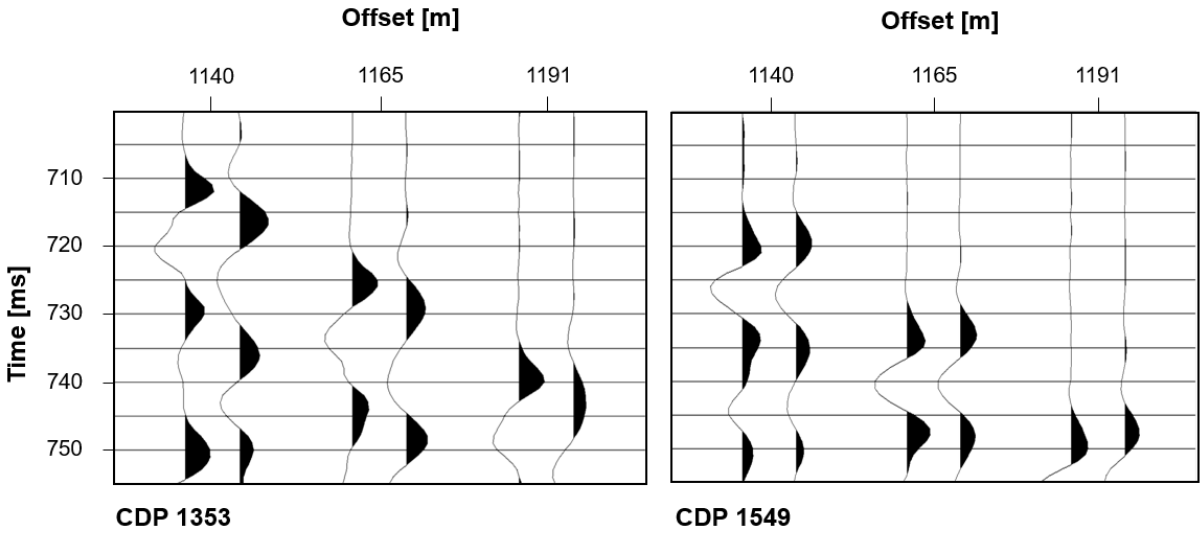

Figure 6.6.3: *Refraction time-shift in alternated trace pairs from 1990 (base) and 2009 (monitor). To the left, CDP location far from the well in SE direction is demonstrated. To the right, CDP location close to the well is displayed. The y-axis is travel time in ms and is the same in both figures.*

Figure 6.6.4 demonstrates the time-shift results for Refraction 1 at 1191 m offset, where the 1990-data is cross-correlated with the data from 2009. A negative time-shift anomaly can be observed, with a decrease in travel-time from 1990 after the blowout to 20 years later. The extent of the anomaly is nearly 1.5 km, reaching about 0.7 km in both southeast and northwest direction from the well. Its maximum negative peak approximately -3.75 ms about 200 m NW of the well. There is some scattering of the data, which is probably due to noise, processing and repeatability issues. These are not considered to be significant time-shift anomalies.

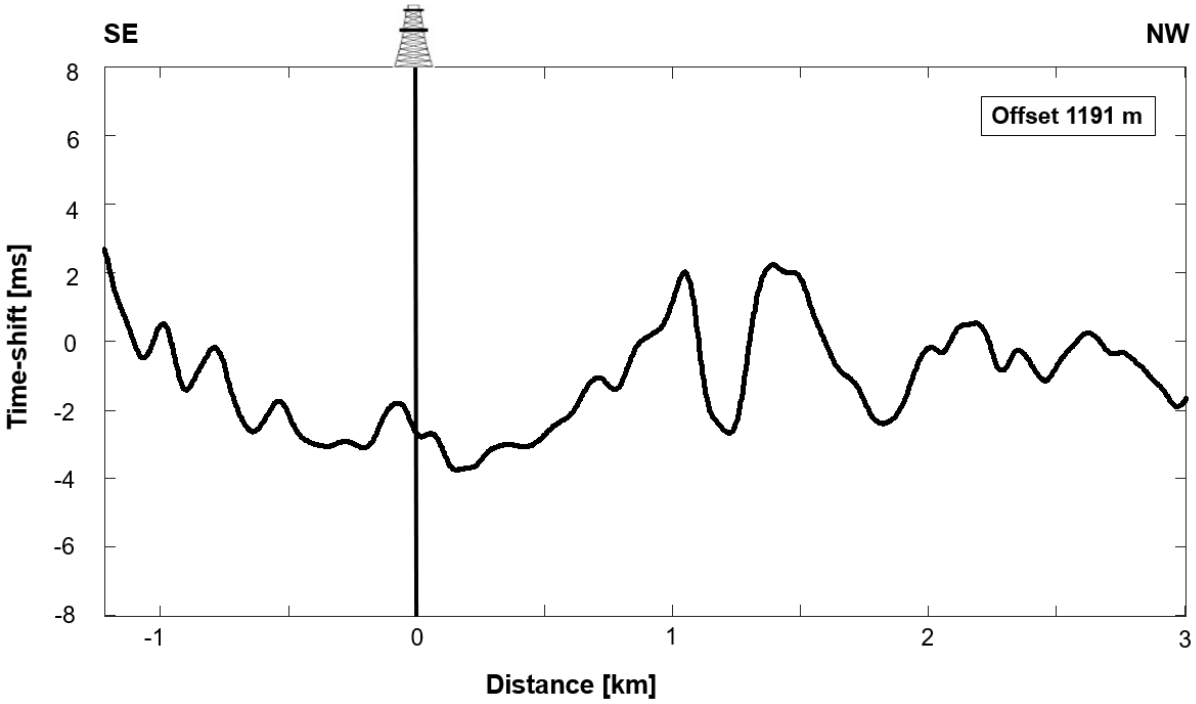

Figure 6.6.4: *Time-shift results for the 1990-data cross-correlated with the 2009 data at offset 1191 m, in relation to the well. A negative trend is observed.*

The procedure of alternating traces for 1988 (base) and 2009 (monitor) is presented in Figure 6.6.5. For both locations, far from the well and in close proximity to it, the traces are nearly aligned in time. However, a slight pull-down effect may be noticed yielding a time-shift of nearly 2 ms.

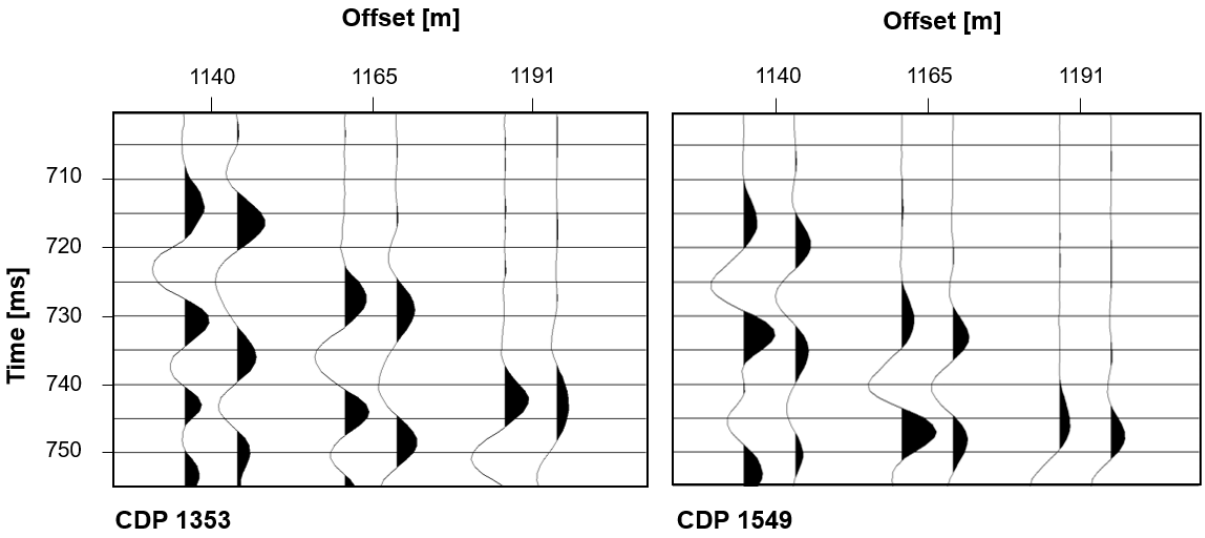

Figure 6.6.5: *Alternated trace pairs from 1988 (base) and 2009 (monitor). Nearly no significant time-shift is observed, and the figures are quite similar.*

Furthermore, cross-correlated time-shift results for 1988 and 2009 is presented in Figure 6.6.6. Smaller peaks are observed across the well and in a northwest direction, with maximum peaks in time-shift at 2.6 and 2.7 ms. Another increase in time-shift is observed nearly 1.5 km northwest from the well but is probably related to some sort of noise. Elsewhere, the trend is generally flat.

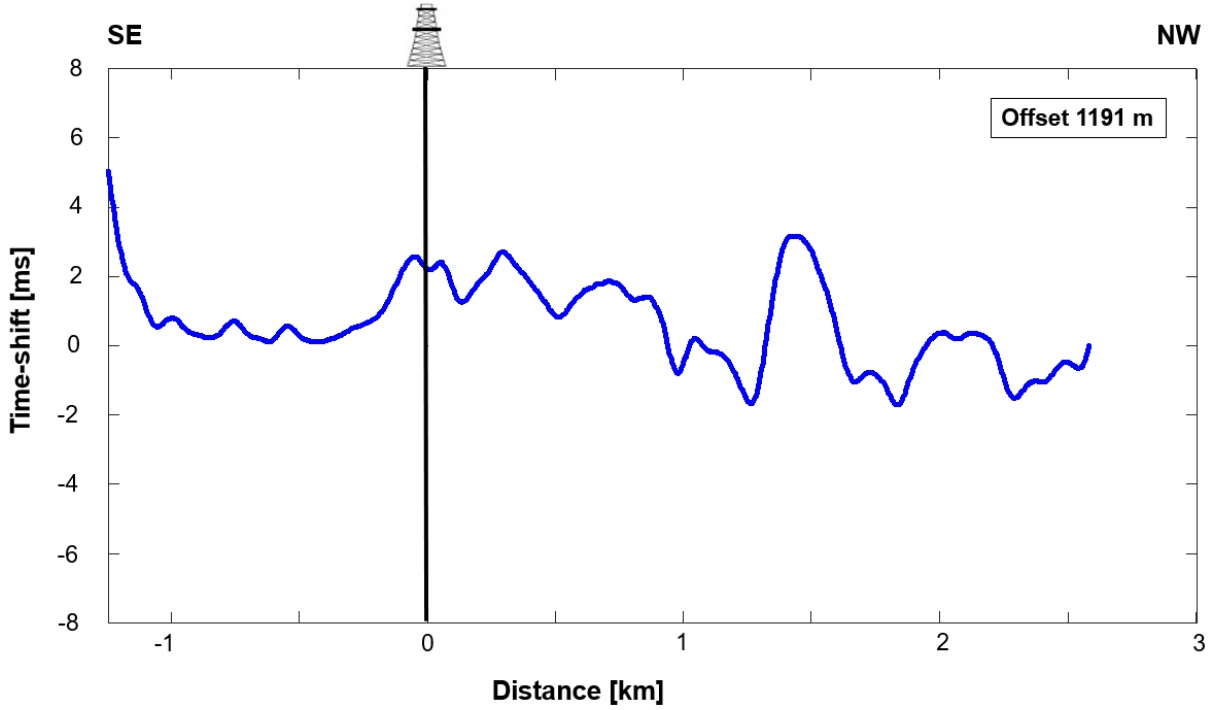

Figure 6.6.6: *Time-shift results of the cross-correlated data, at offset 1191 m, from before the blowout and 20 years later.*

Figure 6.6.7 presents the development of the anomaly over calendar time, from before the blowout and until 20 years later. The three cross-correlations are combined and it is clear that the main anomalies are located in the same area and gives a better overview of the results for further interpretation. The anomalies correlate well with each other, indicating a pattern where the anomalies clearly match in location. The red line is the cross-correlation of the 1988-1990-data, from before and after the blowout, demonstrating a positive anomaly. The black line shows the cross-correlation now from the 1990-2009-data, showing a negative anomaly, and the blue line is the 1988-2009 data presenting a relatively flat trend. Discrepancies are observed on both sides in southeast and northwest direction from the well.

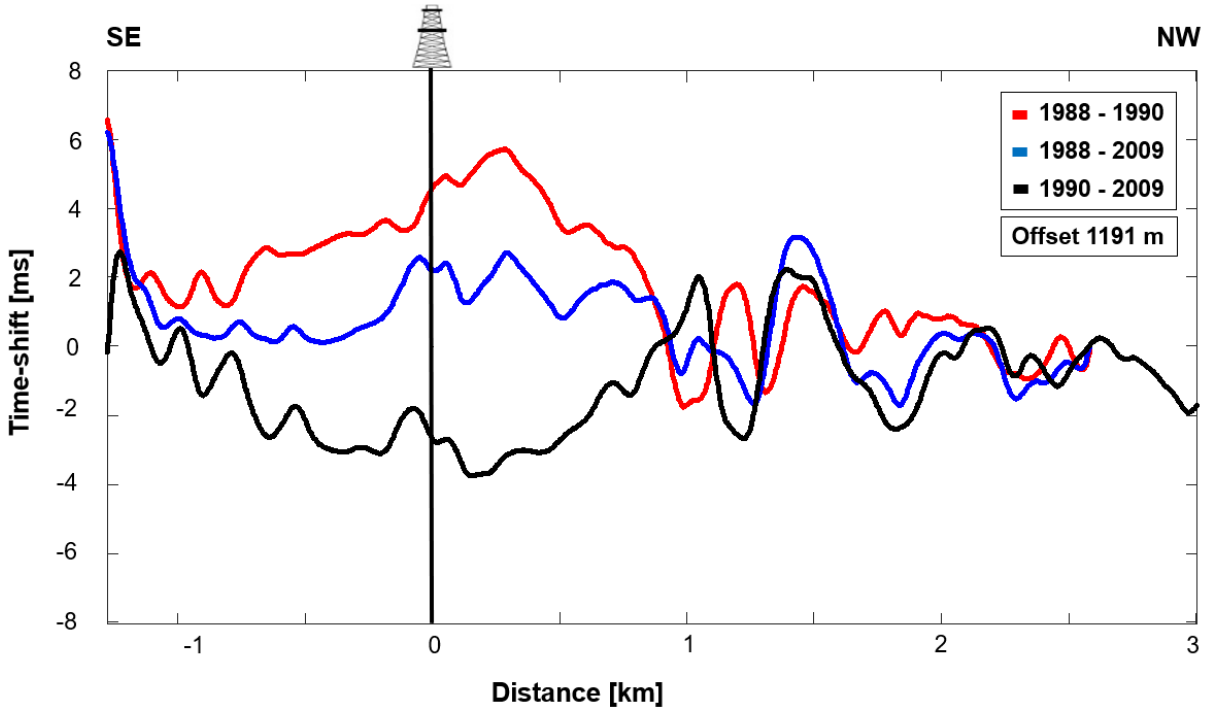

***Figure 6.6.7**: Cross-correlated time-shift results of all three datasets for offset 1191 m.*

The anomaly clearly visible in Figure 6.6.7 is linked to previous research done by Zadeh and Landrø (2011), where the anomaly was calculated to correspond to 220 ms and at an estimated depth of 165 – 175 m. Moreover, the data is analyzed at shallower depths of the subsurface by looking for anomalies for offsets as short as possible.

6.7 Time-shift Results for Refraction 2

To search for anomalies at shallower depths, shorter offsets are investigated. The results in this section show the cross-correlation for Refraction 2, processed with the same time-gate and time-window, all for 515 m offset.

The alternation of trace pairs regarding the 1988 and 1990 data for Refraction 2 is displayed in Figure 6.7.1 for offsets 491 m to 540 m. Again, to the left in these trace plots, CDP locations nearly 2 km SE of well 2/4-14 is presented. Keeping in mind the 3 ms displacement, no significant changes in time are observed. To the right, traces located approximately 200 m NW of the well is shown. For offsets 515 and 540 m, the traces are nearly aligned, yielding a positive time-shift of nearly 3 ms. When comparing the traces with the analysis of Refraction 1, the data quality is observed to be more influenced by noise.

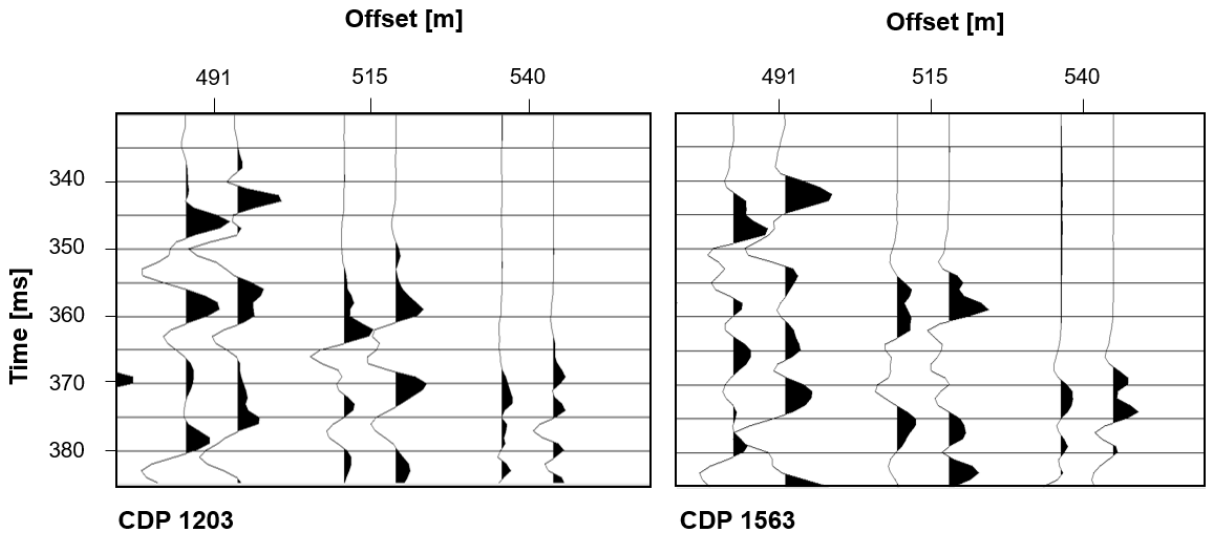

Figure 6.7.1: *Refraction time-shift in alternated trace pairs from 1988 (base) and 1990 (monitor). To the left, CDP location nearly 2 km SE of the well is presented. On the right-hand side, CDP location approximately 200 m NW of the well is displayed. The y-axis is travel time in ms and is the same in both figures.*

The cross-correlation of the 1988 and 1990 data for Refraction 2 at 515 m offset is presented in Figure 6.7.2. The results show two anomalies. The first anomaly intersects the well, with an increase in time-shift reaching a maximum at 3.27 ms and a lateral width of approximately 1.1 km. The second anomaly starts approximately 0.75 km northwest of the blowout well and is somewhat shorter in lateral extent, with a width of nearly 0.65 km and with a maximum peak of 2.17 ms. What may be a third anomaly is observed 2.5 km from the well, following a section with a more negative trend. The anomaly is small in extent, only 0.3 km and 1.1 ms in maximum time-shift.

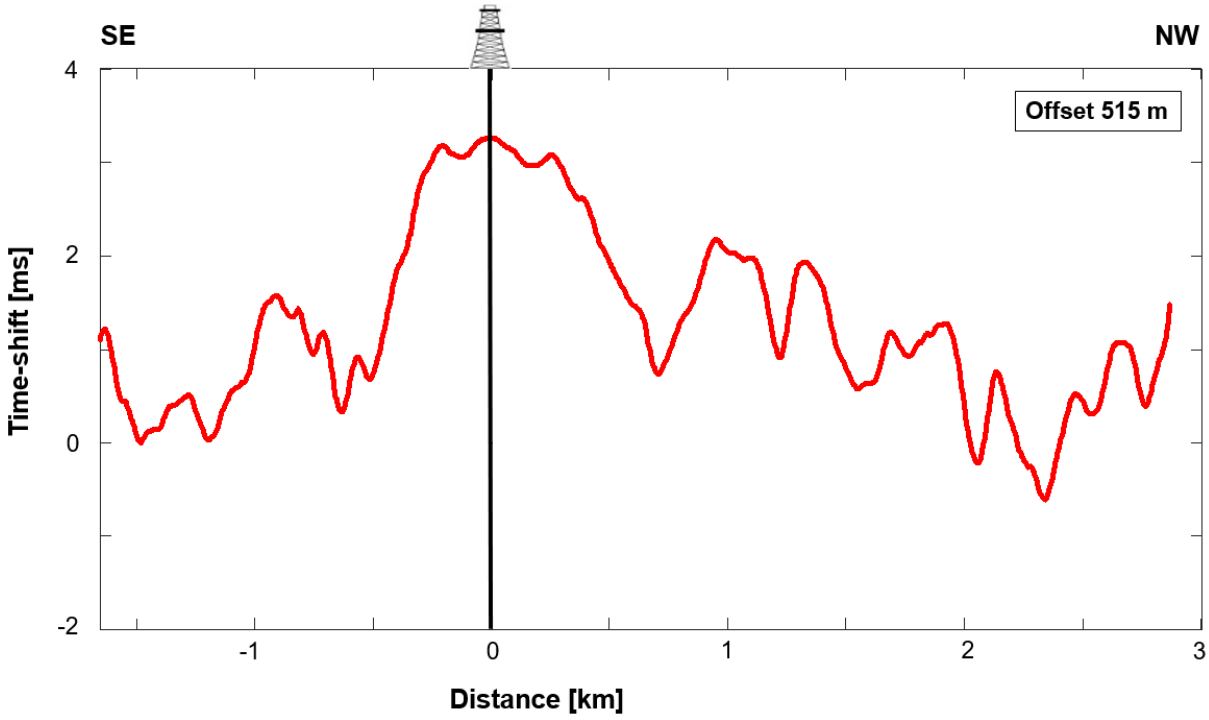

Figure 6.7.2: *Cross-correlated time-shifts of the 1988 and 1990 data for refraction 2 at offset 515 m, in relation to the well.*

Trace plots with 1990 as base and 2009 as monitor are displayed in Figure 6.7.3. To the right, close to the well, a negative time-shift of nearly 3 ms is observed. This is only noticed for offset 515 m.

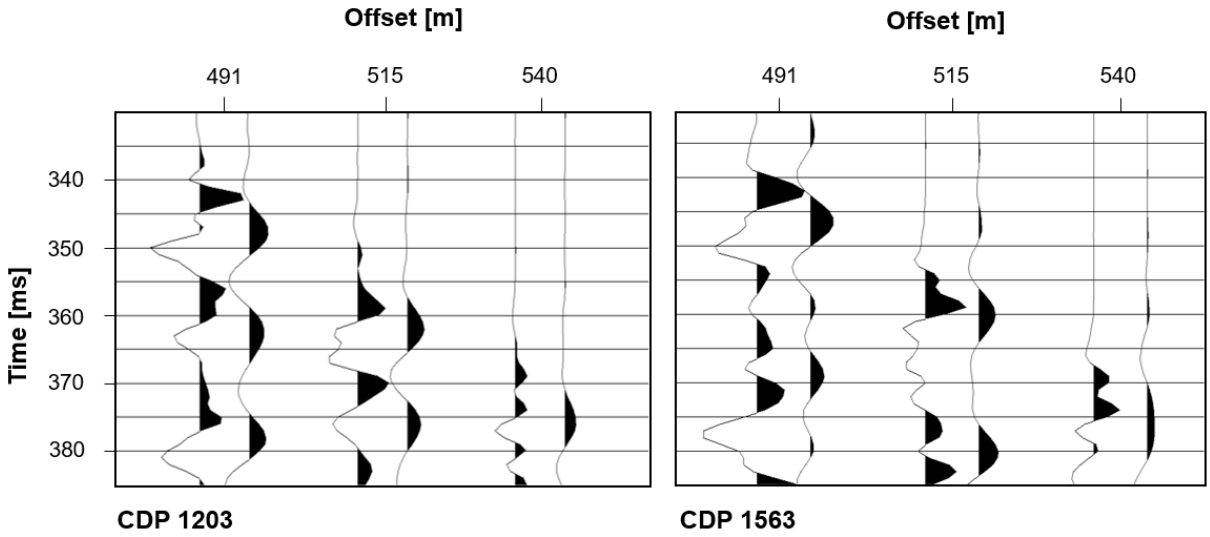

Figure 6.7.3: *Refraction time-shift in alternated trace pairs from 1990 (base) and 2009 (monitor). To the left, CDP location nearly 2 km SE of the well is presented. On the right-hand side, CDP location approximately 200 m NW of the well is displayed.*

The resulting time-shift values plotted in MATLAB for correlated 1990 and 2009 data at 515 m offset is presented in Figure 6.7.4. There is a clear negative trend, almost mirroring the results in Figure 6.7.2. A negative anomaly is observed of approximately 1.1 km intersecting the well with a maximum peak of approximately -3.16 ms. A second negative trend with a maximum negative peak at -2.14 ms is observed ca. 1 km northwest of the well. The trend is elsewhere focused around zero ms.

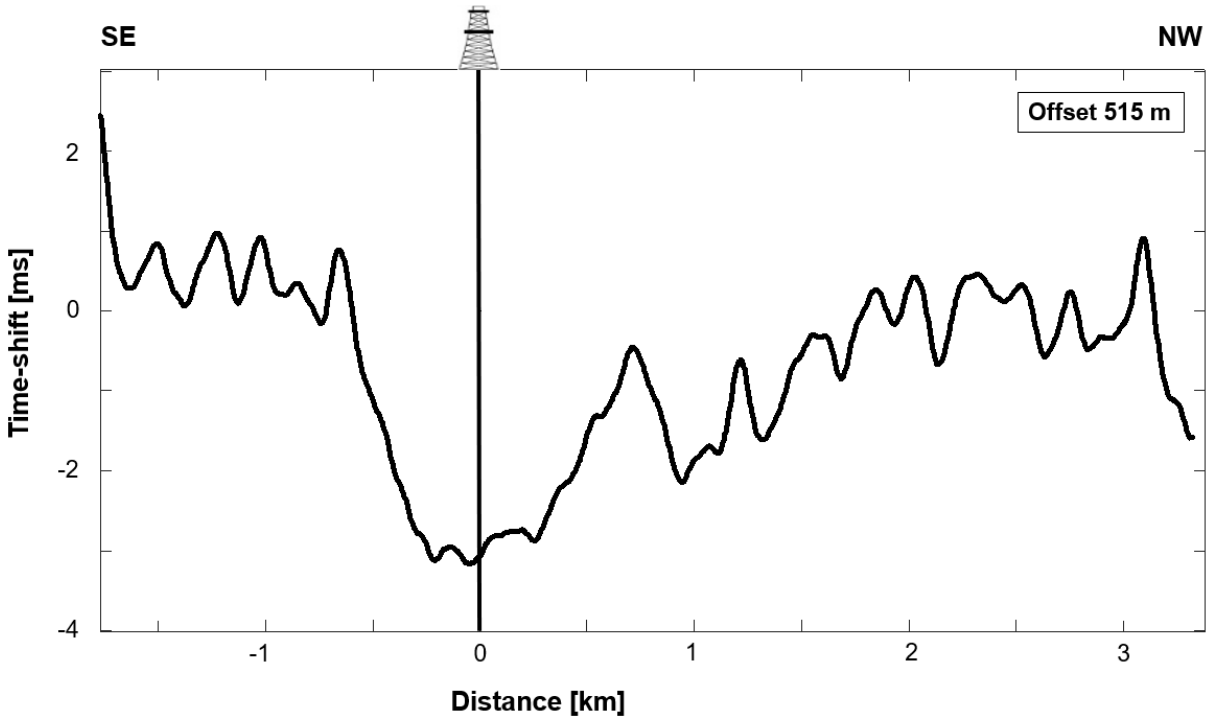

Figure 6.7.4: *Cross-correlated time-shifts in ms of the 1990 and 2009 data, for offset 515 m in relation to the well.*

Trace plots from the alternation of 1988 and 2009 data are shown in Figure 6.7.5. Especially for offset 515 m, it is observed that the traces are aligned in time both for 1988 and 2009 data. Note that the 3 ms displacement is not present in this figure.

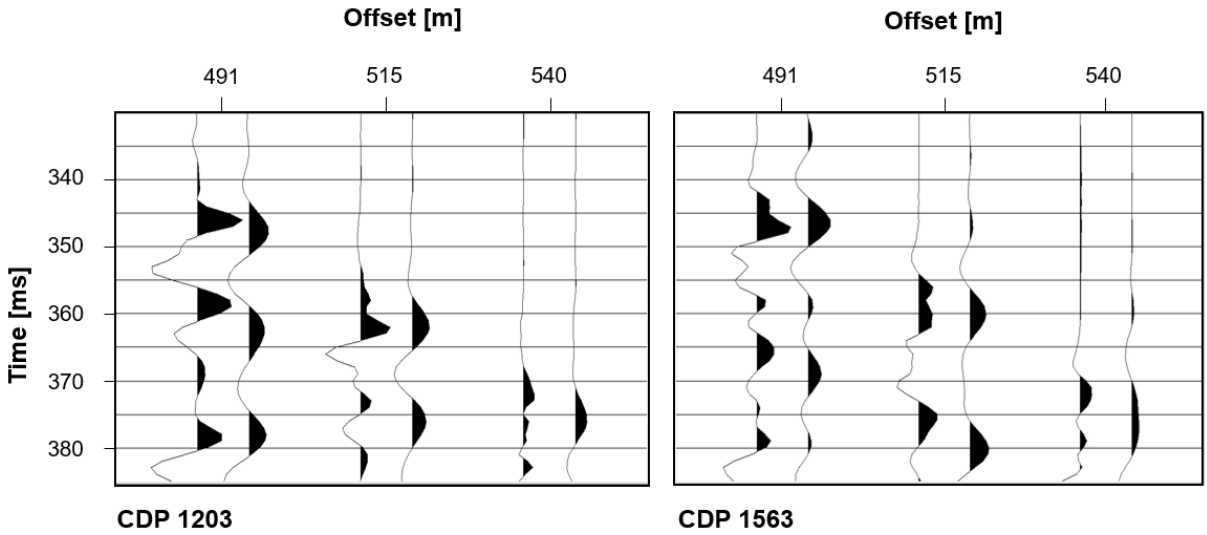

Figure 6.7.5: *Refraction time-shift in alternated trace pairs from 1988 (base) and 2009 (monitor). To the left, CDP location nearly 2 km SE of the well is presented. The trace pairs are aligned in time, yielding no time-shift in both figures.*

The results from cross-correlating the 1988 and 2009 data for 515 m offset is presented in Figure 6.7.6. As in the trace plot, no significant anomalies are observed, and the trend remains stable around zero time-shift. In the southeast direction from the well, some fluctuation probably related to noise is observed, and some indications of a positive time-shift trend can be observed from approximately 2 km in the further northwest direction from the well.

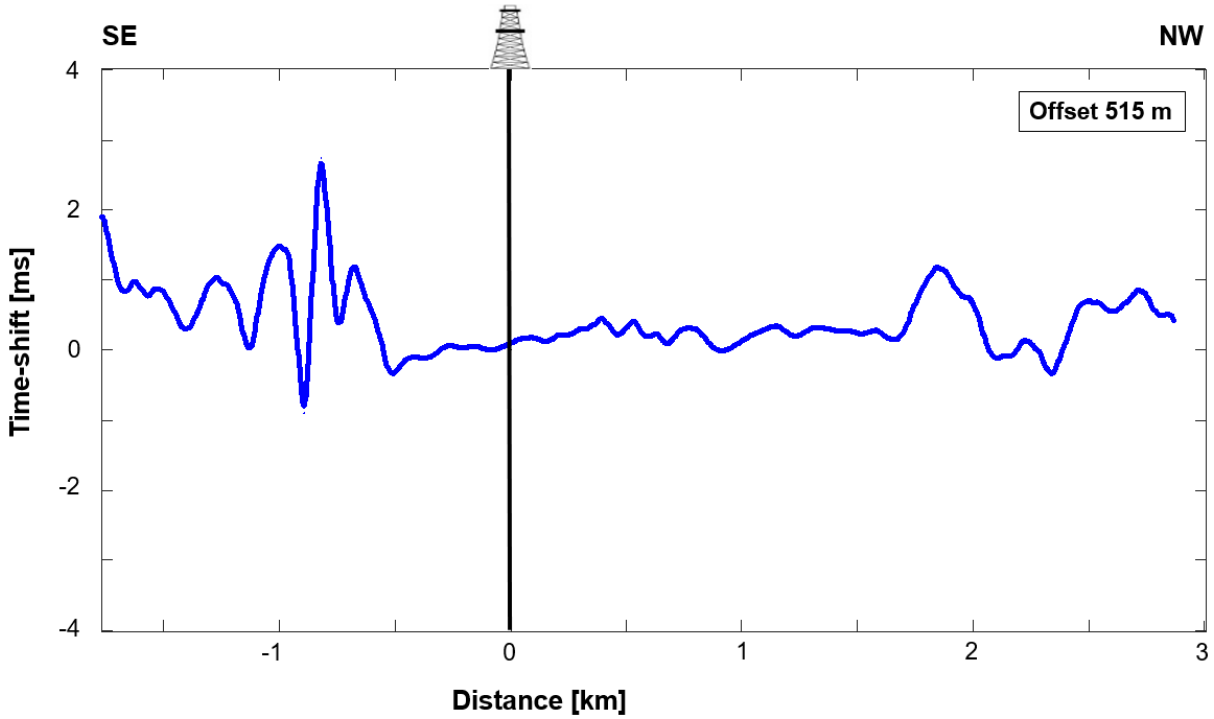

Figure 6.7.6: *Cross-correlation of the 1988 and 2009 data, for offset 515 m, in relation to the blowout well.*

When the three time-shift results are plotted together, as shown in Figure 6.7.7. The development of the anomaly can be seen in relation to calendar time. It is apparent that the results and anomalies correlate for the same locations across the 804 line. The red line shows the results before and after the blowout, with clear positive anomalies. The black curve shows the cross-correlation of the 1990 data and the survey acquired 20 years after the blowout, showing significant negative trends. The blue curve is the data from before the blowout cross-correlated with the 2009 data, which results in nearly no response on the time-shift scale, with the trend focused around zero. Fluctuations in time-shift response, probably related to noise, are present on both sides SE and NW of the anomalies.

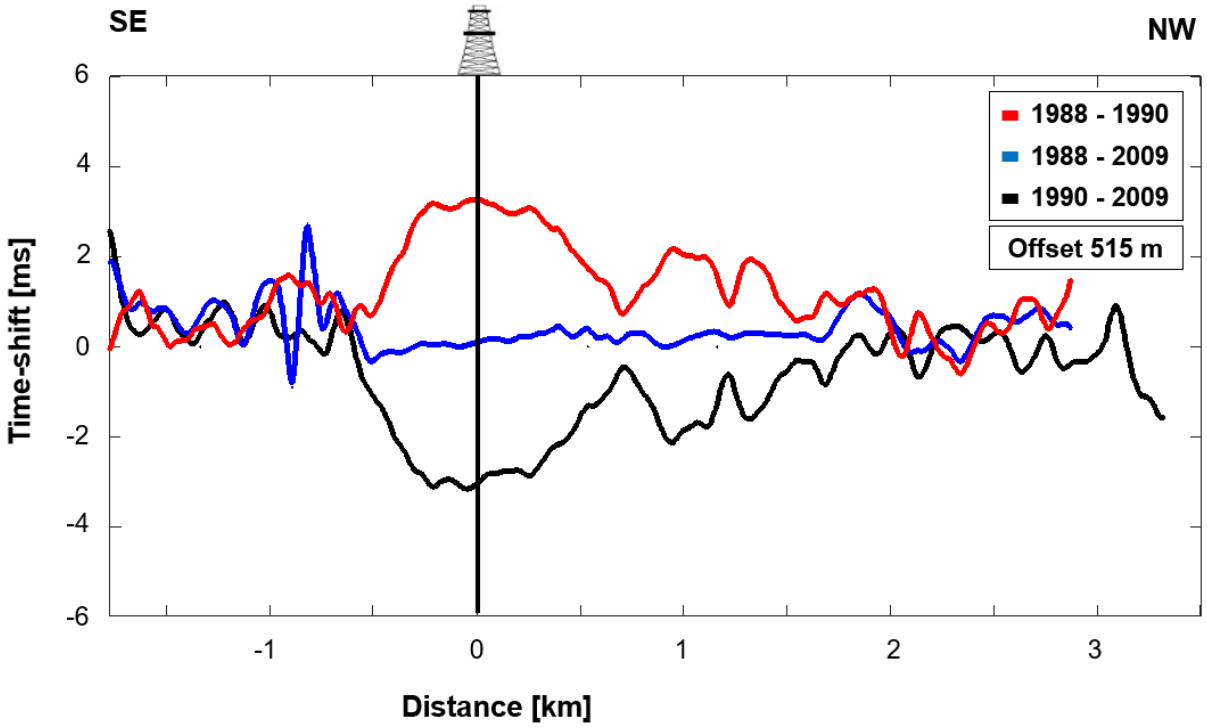

Figure 6.7.7: *Cross-correlation for all three datasets at offset 515, showing the development through time from 1988 to 2009. At least two anomalies are clearly visible, with a flat trend in the middle.*

By picking different time-gates, as well as varying the offset, the results differ. Figure 6.7.8 demonstrates these changes in time-shift as the offset increases and the time-gate is kept constant, for the cross-correlation between the 1988 and 1990 data. The offsets range from 503 to 566 meters and are marked in different colors as seen in the legend. For larger offsets, the third trend described in Figure 6.7.2. becomes more distinct, the second trend however weakens. The anomaly intersecting the well remains approximately the same. Figure 6.7.9 presents the changes in time-shifts for different picked time-gates, where the offset is kept constant at 540 m. The figure only demonstrates the cross-correlation performed on the 1988 and 1990 data. The length of the time-window is set to 19, 12 and 17 ms for time-gates 1 to 3, respectively.

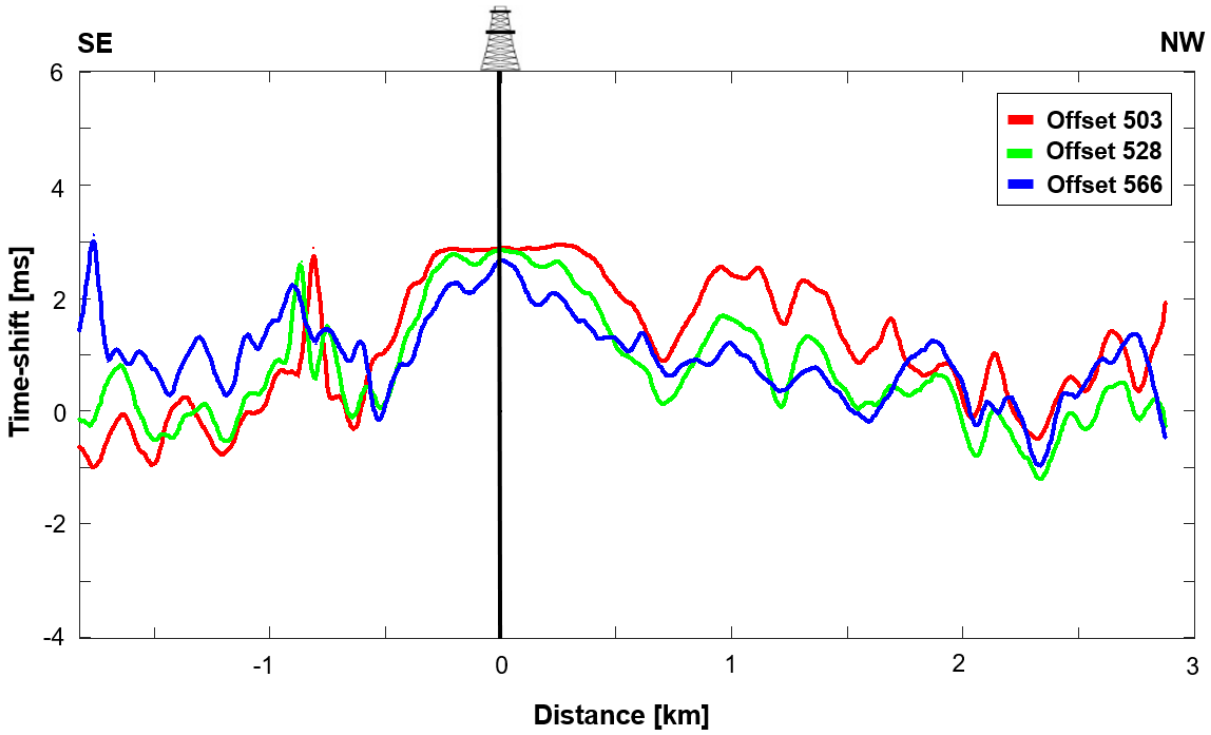

Figure 6.7.8: *Cross-correlation of the 1988 and 1990 seismic data, for the same time-gate but with variations in offset from 503 m to 566 m.*

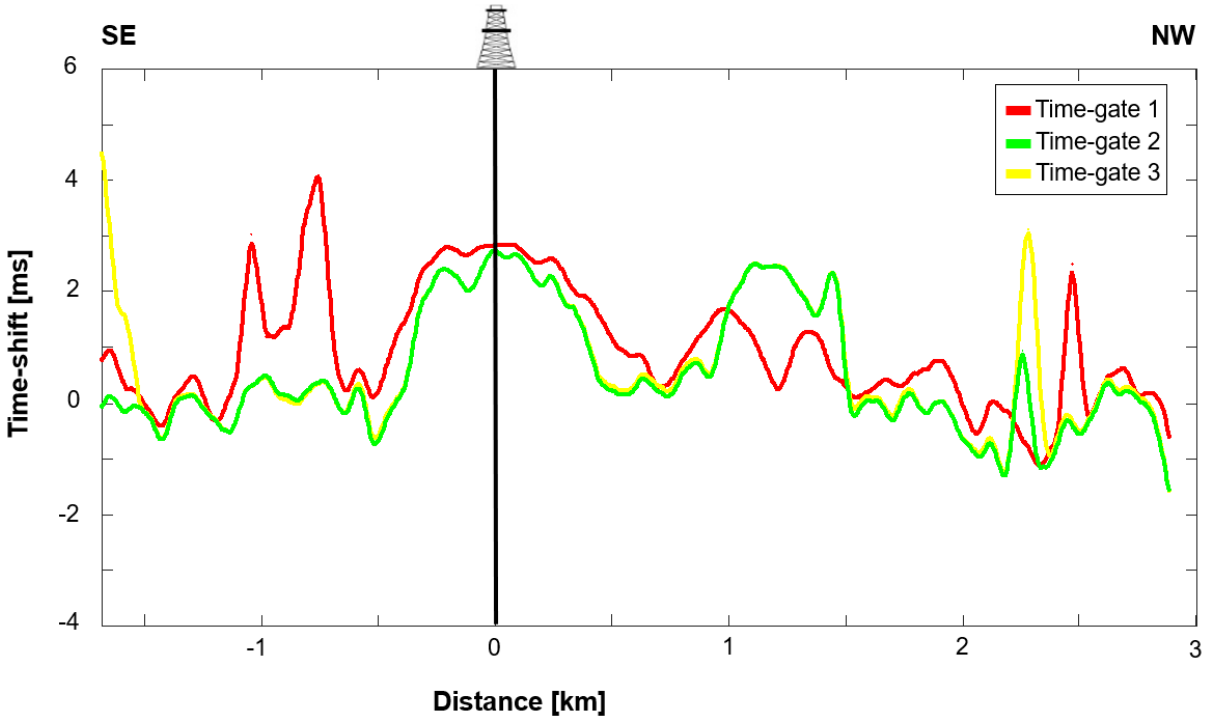

Figure 6.7.9: *Changes in time-shift results for different picked time-gates. The offset is kept constant at 540 m. The length parameter for time-gates 1 to 3 is 19, 12 and 17 ms, respectively.*

When combining the above results from the cross-correlation of Refraction 2 with the brute stack, the anomalies gives a conspicuously good correlation with the interpreted tunnel valleys, as seen in Figure 6.7.10. The x-axis for the stack and the time-shift results have been matched and show the distance in relation to the well. The y-axis is however not the same, with time-shift in ms on the upper left part of the figure and travel time in ms in the lower right part. It is observed that the two anomalies correlate well both in estimates of depth and in lateral extent.

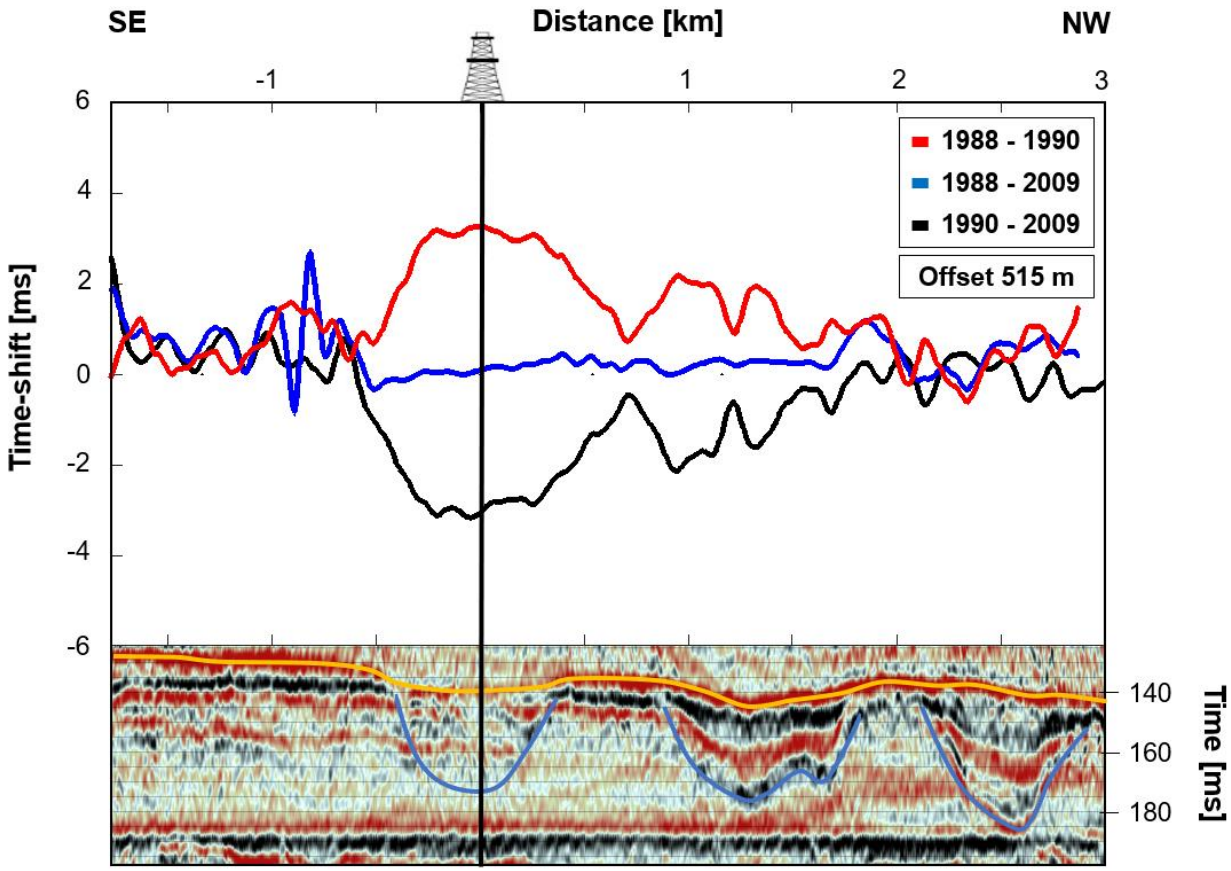

Figure 6.7.10: *Cross-correlated time-shift results for all three datasets for refraction 2, at offset 515 m, compared with the brute stack from 1988 corresponding to the seismic line 804. The tunnel valleys are interpreted and marked with blue lines, while the top of the layer is marked in yellow. Well 2/4-14 is indicated with a black line.*

6.8 Estimates of Depths and Velocity

The slope of Refraction 2 is estimated in ProMAX to an average velocity of 1763.4 m/s. The intercept is then estimated to 0.365 s. Simple calculations lead to an estimated average value of t_0 to be 0.0639 s. The depth of the refraction interface can then be calculated, given that the velocity above and below the interface is known. By using equation (6) and assuming V_1 to be 1600 m/s and V_2 to 1763.4 m/s, the depth of the refraction anomaly at 515 m offset is calculated to approximately 121.6 m depth. The depth of the water layer is 68 m, hence the depth of the refraction interface is 53.6 m below the surface.

The velocity of the water layer is assumed to be 1500 m/s. Given the water depth of 68 m and that the depth from the first layer to the interface is 53.6 m, the reflection travel-time is calculated to 157.6 ms.

By using equation (10) and the observed maximum time-shifts, the change in velocity can be estimated. For the anomaly intersecting the blowout well this gives a velocity decrease of 9.36 m/s for 1988 to 1990, and a velocity increase on 10.5 m/s from 1990 to 2009. For the anomaly further northwest of the well, an estimated velocity decrease of 8.3 m/s and an increase of 8.4 m/s from 1988 through to 2009. It should be emphasized that these calculations are only estimates.

7 Discussion

The overall variance in time-shift computed by cross-correlating refracted waves from repeated seismic as described in the above sections suggests the following. A decrease in velocity through a layer will lead to an increase in travel time, hence a positive time-shift from base to monitor data. An increase in velocity through a layer for one seismic dataset to another will result in a decrease in travel time for the refracted wave, hence a negative time-shift is computed. No response in time-shift, where the trend is relatively stable and centered around zero, indicates the same velocity in the layer for the base and monitor data. From reservoir physics with regards to the Gassmann model, a change in velocity may indicate a change in pore fluids, which in this case is probably due to gas with a view to the underground blowout that occurred in 1989.

7.1 4D Time-shift Analysis of Refraction 1

Figure 6.6.7 demonstrates the cross-correlation of Refraction 1 for all three datasets for offset 1191 m. The red line represents the time-shifts before and after the blowout, from 1988 to 1990 respectively, showing a distinct anomaly with a maximum peak of ca. 5.7 ms. Due to the blowout in well 2/4-14, it is reasonable to interpret this positive time-shift being caused by gas migrating vertically into shallower layers. The further development of what may have happened to the gas between 1990 and 2009 is demonstrated with a black line, resulting in a negative time-shift, with a peak of approximately -3.75 ms. This indicates less gas in 2009 than it was in 1990 after the blowout. This is as expected, and one may interpret some of the gas to be slowly diffusing through the silt and sand layers present in the area. On the contrary, a positive time-shift would have indicated an increased supply of gas. Nevertheless, it is noted that the negative time-shift has a lower absolute value than the positive time-shift, supporting the interpretation. The cross-correlation between the 1988 and 2009 data indicated by the blue line shows a relatively flat trend, however, a slight positive response with several peaks of nearly 3 ms is observed. This result supports the interpretation, as it indicates more gas in 2009 than it was in 1988. It may be interpreted that the gas at this level is relatively stable and remains nearly the same.

The trace plots present the alternation of trace pairs between the base and monitor data for the three surveys at offsets 1140 to 1191 meters. The figures are interpreted by looking at the changes in travel time from base to monitor, showing either a pull-up, a pull-down or no change

at all. This alternation of traces is also seen in context from far away from the well where no gas anomalies are expected and closer areas intersecting the blowout-well where gas anomalies may be detected. When analyzing these figures, it is important to note that there is an already 3 ms displacement in the 1990 data which is corrected for in MATLAB when creating the time-shift plots. The increase and decrease in travel time for the chosen areas correlate well with the observed time-shift anomalies in the cross-correlated time-shift plots for the corresponding data.

In Figure 6.6.7 it is also observed that both the positive and negative observations of the gas anomalies occur with approximately the same lateral extent located around the well area. For both the negative and positive time-shift anomalies, the extent is approximately 2 km. The anomalies represented by the blue line has an extent closer to 1 km and in more of a northwest direction from the well location. Nevertheless, all three lines have a response within the same area.

Previous studies by Zadeh and Landrø (2011) performed on what is assumed to be the same anomaly, calculates the depth of the possible refraction anomaly to about 165-175m, corresponding to 220 ms in two-way travel time, yielding a velocity decrease of approximately 25 m/s in the blowout area. These estimates are hard to quantify without knowing the velocity model at the field location, in addition to this, there is no sonic log available in these shallower areas to quantitatively confirm or refute both depth and velocity of the potential sand layers serving as hosts for gas accumulations.

7.2 4D Time-shift Analysis of Refraction 2

The analysis of the second refracted event is at a lower offset, indicating shallower depths. The refraction was investigated from approximately 491 to 853 meters in offset and shows the shortest offset possible to interpret throughout this study. Anomalies in time-shift response are most clear at offsets from 515 to 540 meters.

Figure 6.7.7 demonstrates the cross-correlation of all three datasets at offset 515m. As for Refraction 1, the red line represents the time-shifts from the pre-drill survey in 1988 and the survey acquired in 1990. At least two clear anomalies are observed, the first anomaly intersecting the well location and the second anomaly appears approximately 750 m northwest of the well. A third and smaller anomaly may be interpreted approximately 2.5 km in the northwest of the well, with a negative trend observed in SE direction of this anomaly. This trend

may be more visible in Figure 6.7.8 which displays the changes in results in relation to applying different time-gates. Several speculations can be made of why this negative trend appears in advance, but it may indicate that the maximum time-shift should be higher. It may be noted that this anomaly coincides with the third tunnel valley in the northwest direction. However, the anomaly is considered below noise level and is not included in this thesis as a significant anomaly.

The positive time-shift anomaly intersecting the well has an observed extent of approximately 1.1 km reaching a maximum time-shift of ca. 3 ms. This is the anomaly with the largest extent, hence it is interpreted that most of the gas is set in this area. The second anomaly with appears smaller both in lateral extent and maximum time-shift values. The occurrence of these anomalies coincides with the time of the blowout event and it may be reasonable to interpret the gas migrating along the well, through the sediments weakened due to drilling, as well as migrating laterally into the porous and permeable tunnel valleys in the area.

The black line in Figure 6.7.7 represents the time-shift results from the cross-correlation between the 1990 and 2009 data. Again, negative time-shift anomalies are observed, and it is noted that these are nearly mirroring the positive trend, which can imply the gas migrating out of the tunnel valleys. It may be suggested that the gas has either leaked further towards the surface and possibly into the water layer, or it may have been transported laterally in the tunnel valley system. The blue line representing the time-shift tendency from before and 20 years after the blowout shows nearly no response and is focused around zero. This result indicates that there is the same amount of gas in 2009 as in 1988, supporting the interpretation of the gas migrating out of the tunnel valleys. Through time, the time-shifts shows an increase in travel time from 1988 to 1990 followed by a decrease back to pre-drill values in 2009.

The trace plots with alternating base and monitor data for the three surveys at offsets from 491 to 540 meters demonstrates the differences occurring in calendar time, seen in context with distances in a southeast direction away from the well and for locations closer to the tunnel valley system and the blowout well. The changes in travel time are in accordance with the results in the time-shift plots for the corresponding data.

By contrast to Refraction 1 at greater depths, it is noted that the data quality at shallower depths produces a noisier amplitude. This accentuates the differences in depths and highlights the

issues with analysis of shallow seismic. As previously mentioned, the seismic data is not acquired with the purpose of shallow analysis performed at the depths done in this study.

Lower magnitude of the amplitudes in Refraction 1 in relation to Refraction 2 is observed when comparing the chosen refractions. This may be reasonable as they are of higher offsets and at greater depths, indicating more damping of the signal. At such shallow depths as investigated in this thesis, it may be noted that to discriminate between diving waves sand refracted waves in field data is problematic. Both diving waves and refracted waves require large offsets to be detected and is why they are often put into the same category. The possibility of the assumed refracted wave might actually be a diving wave is noteworthy. Nevertheless, the time-shift results are still significant, regardless of being due to refractions or diving waves.

7.3 Refraction Time-shifts in Comparison with Stacks

When the anomalies for Refraction 2 are compared with the stack as presented in Figure 6.7.10 and seen in relation with estimated depth and lateral extent, the anomalies correlate remarkably well with the interpreted tunnel valleys. The areas between the anomalies have no significant response in time-shift, as expected when seen in relation to depressions in the stack. Comparing estimations of reflection travel time and depth with the stack this is also in accordance with the interpreted tunnel valleys.

The stacks shown in Figure 6.5.1 and Figure 6.5.2 can also give indications supporting the interpretations. With a view to the structure and sediment infill of tunnel valleys, often having high permeability and porosity, they provide good potential as hosts and flow paths for fluids. Several cut-and-fill structures might enable the valleys to transport fluids. Figure 6.5.2 displays a closeup of the reflection data from 1988 to 2009, as well as a difference section from before and after the blowout. There is a brightening in the tunnel valleys northwest of the well, especially on the edges, and may be interpreted to be caused by gas. Upon comparison, the tunnel valley intersecting the well has a more scattered reflectivity pattern, indicating a more heterogeneous infill being chaotic and less organized, where the gas may float more out. This underlines the strength of using 4D refraction seismic, where the horizontal waves enable us to detect velocity changes that are not always as clear in regular reflection seismic. The other tunnel valleys appear to have greater inner structure and seem to be more layered. Here, the anomalies show a lower response and the layering may act as barriers to the gas.

In relation to the whole, both results from Refraction 1 and 2 may indicate that the hydrocarbons migrating from the blowout both vertically and laterally, accumulating in the shallow sand layers and tunnel valleys. Thereafter, it seems like the gas has migrated out of the tunnel valleys as seen in the negative time-shift anomalies. The gas may have diffused through the silt and clay packages and towards the surface, or it may have proceeded laterally in the tunnel valley system that covers a large area. A combination of both is also suggested. At the well location, a leak might be possible. Nevertheless, the tunnel valleys may also be preventing leakage into the water layer.

Previous studies of the shallow subsurface in this area have also resulted in the interpretation of occurrence of shallow gas, where ice scours function as traps for naturally occurring gas (Haavik, 2012). From reservoir physics, in the view of the Gassmann model, a velocity decrease is not necessarily due to changes in fluid saturation. Alternations in velocity in a layer can, for example, be due to decompaction, temperature decrease, porosity increase and other structural changes occurring in the area.

Figure C1 shows research by Martin Landrø on reflection time-shifts from the same seismic site survey, across line 804. The figure illustrates reflection data from 1988 to 2009, where the seabed has been aligned to 100 ms. It is observed a significant increase in time-shift between the 1988 and 1990 data close to the well, followed by a reduction back to pre-blowout values in 2009. These 4D reflection time-shifts are concordant with the 4D refraction time-shifts, at least on a qualitative level.

7.4 Uncertainties and Repeatability

The method enables energy to be observed at shorter offsets and shallower depths. A response in velocity differences caused by changes in fluids can be obtained over structures that are not necessarily detected by the use of conventional seismic reflection methods. By using 4D refraction time-shifts as a method to analyze the shallow subsurface involves several uncertainties and limitations that will be addressed in the following section.

Generally, in order to generate either refractions or diving waves, an increasing velocity earth is required. This is one of the practical disadvantages of the time-lapse refraction method, limiting the number of shallow interfaces where these types of waves may occur.

4D seismic methods are also dependent on repeatability, including several factors for instance temperature changes, weather conditions, tidal effects, acquisition equipment as well as the direct effect random noise can have on the time-shift values. Another factor that may confirm or refute the interpretation, is the correlation between anomalies and source coordinates during acquisition. Figure 6.1.2 and Figure 6.1.3 shows the x-and y-coordinates for shot-positions during acquisition of the surveys. A difference in source coordinates could possibly have an effect on the travel times, leading to an anomaly. As observed in Figure 6.1.4 there exists a shift in the 1990 data of approximately 3 ms and may have an impact on the results.

Figure 6.1.2 is displayed together with the estimated extent of anomalies discovered in Refraction 2. No significant consistencies between the anomalies and positions are observed and are also supported by the approximated absolute values for the differences between 1990 and 1988 source coordinates as displayed in Figure 6.1.3. This supports the interpretation of the anomalies being caused by gas in the tunnel valleys rather than due to an acquisitioning error. Still, since the source positions from the 1990 data appear in a very straight line, the coordinates might reveal to be the desired coordinates and not the true measurements. This can have an impact on the validity of the results. For the vessel to sail in a completely straight line is unattainable, however, the likelihood of the vessel sailing in a deviant matter to coincide with the exact extent of the tunnel valleys seems very small.

In the area, it is also known to be a dip in the layers, but at the shallow depths investigated in this thesis, this dip should not be able to have the effect of generating the significant anomalies observed.

There is also a level of uncertainty regarding the repeatability of the 2009 data, as it is acquired in the opposite direction than the other two surveys. Nevertheless, by processing the data in the CDP-domain rather in the shot-domain, this still yielded the same results. Uncertainties regarding the processing of the datasets may also have an impact on the results. On the 1988 and 1990 data, limited processing has been performed in order to reduce the noise level or to remove multiples. On the 2009 data, however, a bandpass-filter was applied prior to the analysis and stabilized the cross-correlation time-shift results.

The time-gates used in this thesis were picked manually for each refracted event, and the time-window was tested to estimate what could include most of the signal. This technique is in general not very accurate and was performed several times until reaching the results, with

varying success. To achieve more accurate results, a more precise processing of the data as well as increasing the signal to noise ratio could be done. Figure 6.7.9 displays some of the uncertainties regarding the picking of time-gates and the adjustments of the time-window. The trend, however, is the same, showing a significant time-shift correlating well with the tunnel valleys. These results highlight some of the uncertainties with the method, as well as it also accentuates some of the anomalies.

Conclusions

The history of offshore activity on the Norwegian Shelf is relatively young, yet comprehensive. Events such as the blowout in Well 14 in Block 2/4 are important reminders of the powerful natural forces at play and have been crucial lessons for future activity and development. This thesis analyses three surveys acquired along the seismic 2D line 804 intersecting the well. By implementing a method utilizing refracted waves in a 4D time-shift analysis, anomalies caused by changes in travel time is investigated and monitored. A change in travel time might indicate a velocity decrease caused by changes in pore-fluids, and in this case, probably due to gas.

By utilizing horizontal energy in time-lapse refraction seismic, estimated time-shifts reveals significant anomalies. These anomalies correlate conspicuously well with the depressions interpreted as tunnel valleys on the seismic stack and matches well both in estimates of depth, lateral extent as well as in reflection travel-times. It is interpreted that the increase in time-shift values are caused by gas from the blowout migrating vertically and laterally into the porous and permeable tunnel valleys present in the area. The negative time-shift values indicate that the gas 20 years later has migrated further out of the tunnel valleys. This is supported by the time-shifts obtained when correlating the 2009 data with the 1988 data, showing the time-shift values going back to pre-drill values. It is interpreted that the gas may have diffused through the layers towards the surface, or the tunnel valleys may have transported the gas laterally. The tunnel valley system might act as storage volumes and transport routes for the gas leakage from below. However, these structures may also serve as an extra buffer against leakage to the surface.

The method holds several uncertainties. First, there is the limited number of interfaces where refractions can occur. Then, there is the data quality including effects of noise and uncertainties regarding the data processing. In 4D seismic, repeatability issues are dependent on many factors, the most critical one is the repeatability of source and receiver positions, and the possibility of a geometry issue in the 1990 data is investigated. Variations in offsets, as well as variations in time-gates influence the results.

Estimation of 4D time-shift values for refracted waves can potentially be used as a complementary monitoring method to regular reflection time-lapse seismic, which might be limited at shallower depths and in more complex structures like tunnel valleys. The horizontal travel path of refractions can detect variations in velocities that may not be visible in regular 4D reflection seismic methods.

Bibliography

Anell, I., Thybo, H., & Rasmussen, E. (2007). A Synthesis of Cenozoic sedimentation in the North Sea. *Basin Research*, pp. 154-179.

Arntsen, B. (2015). *Geophysical Analysis.* NTNU.

Avseth, P. (2010). Explorational Rock Physics – The Link Between Geological Processes and Geophysical Observables. In K. Bjørlykke, *Petroleum Geoscience: From Sedimentary Environments to Rock Physics.* Berlin: Springer-Verlag.

Claerbout, J. (2010, November). *Basic Earth Imaging; Seismic reciprocity in principle and practice.* Retrieved from http://sepwww.stanford.edu/sep/prof/toc_html/bei11.2010.pdf

Clark, C. D., Hughes, A. L., Greenwood, S. L., Jordan, C., & Sejrup, H. P. (2010). Pattern and timing of retreat of the last British-Irish Ice Sheet. *Quaternary Science Reviews*, ss. 1-35.

Cofaigh, C. Ó. (1996, March 1). *Tunnel valley Genesis*. Retrieved from Progress in Physical Geography: http://journals.sagepub.com/doi/abs/10.1177/030913339602000101

Deegan, C., & Scull, G. J. (1977). A standard lithostratigraphic nomenclature for the Central and Northern North Sea. *NPD Bulletin 1*.

Encyclopedia.com. (2018, March 11). *A Dictionary of Earth Sciences*. Retrieved from Encyclopedia.com: https://www.encyclopedia.com/science/dictionaries-thesauruses-pictures-and-press-releases/direct-wave

Foseide, B. (2017). *Quantitative Refraction Traveltime Analysis of 3D Seismic Acquired After an Underground Blowout in the Central North Sea.* Trondheim: NTNU.

Geometrics. (2018, February). *Geometrics*. Retrieved from http://www.geometrics.com/what-is-reciprocity/

Grindstad, E. (2017). *AVO Analysis of a thin Gas-Saturated Sandstone Layer and the Impact of Anelastic Attenuation and Tuning on the AVO Response.* Trondheim: NTNU.

Halliburton Landmark. (2017, December 17). *Halliburton Landmark Solutions*. Retrieved from SeisSpace ProMAX: https://www.landmark.solutions/Portals/0/LMSDocs/Datasheets/Seisspace-promax-data-sheet.pdf

Halliburton Landmark. (2018). *ProMAX Reference Manual*.

Halvorsen, H. S. (2012). *Mapping of shallow tunnel valleys combining 2D and 3D seismic data, Master thesis.* Trondheim: NTNU.

Kazei, V., Troyan, V., Kashtan, B., & Mulder, W. (2013). On the role of reflections, refractions and diving waves in full-waveform inversion. *Geophysical Prospecting*, pp. 1252-1263.

Kehew, A. E., Piotrowski, J. A., & Jørgensen, F. (2012). Tunnel valleys: Concepts and controversies- A review. *Earth-Science Reviews 113(1-2)*, pp. 33-58.

Knopoff, L., & Gangi, A. F. (1959, October). Seismic Reciprocity. *Geophysics*, pp. 681-691.

Landmark, H. (2017, December 17). *Halliburton Landmark Solutions*. Hentet fra SeisSpace ProMAX: https://www.landmark.solutions/Portals/0/LMSDocs/Datasheets/Seisspace-promax-data-sheet.pdf

Landrø, M. (2008). *Anvendt geofysikk i TPG4100 Fysikk og Geofysikk.* Trondheim: NTNU.

Landrø, M. (2010). 4D Seismic. In K. Bjørlykke, *Petroleum Geoscience - From sedimentary Environments to Rock Physics* (pp. 427-444). Berlin: Springer-Verlag.

Landrø, M. (2011, June). Seismic monitoring of an old underground blowout - 20 years later. *First Break.*

Landrø, M. (2014). *Underground Blowout NTVA.* Retrieved from NTVA: https://www.ntva.no/wp-content/uploads/2014/01/280610-landro.pdf

Landrø, M., & Amundsen, L. (2017, May). Time-Lapse Refraction Seismic 1 - A Complementary Monitoring Method? *GeoExPro*, pp. 54-56.

Landrø, M., & Amundsen, L. (2018). *Introduction to Exploration Geophysics with Recent Advances.* Bivrost.

Landrø, M., Nguyen, A. K., & Mehdizadeh, H. (2004). Time lapse refraction seismic - A tool for monitoring carbonate fields? *SEG Technical Program Expanded Abstracts 2004*.

MathWorks. (2017, December 17). *MathWorks*. Retrieved from MATLAB Product Description: https://se.mathworks.com/help/matlab/learn_matlab/product-description.html

Mjelde, Ø., & Bakøy, P. (1991). Geology, pressure prognosis and status of knowledge, rock mechanics. *2/4-14 Experience Transfer Seminar*.

NORLEX. (2018, February). *Nordland Group*. Hentet fra http://nhm2.uio.no/norges/litho/nordland.php

Norwegian Petroleum Directorate. (2018, February). *NPD factpages*. Retrieved from http://factpages.npd.no/ReportServer?/FactPages/PageView/strat_Litho_level1_group_formation&rs:Command=Render&rc:Toolbar=false&rc:Parameters=f&NpdId=113&IpAddress=129.241.230.119&CultureCode=en

Norwegian Petroleum Directorate. (2018, April). *NPD Factpages*. Retrieved from http://factpages.npd.no/FactPages/Default.aspx?nav1=wellbore&nav2=PageView|Exploration|All&nav3=1343&culture=en

NPD. (2018, May 15). *Factmaps*. Retrieved from Norwegian Petroleum Directorate: http://gis.npd.no/factmaps/html_21/

Petroleumstilsynet. (2018, May). *Petroleumstilsynet*. Retrieved from http://www.ptil.no/artikler-i-sikkerhet-status-og-signaler-2012-2013/saga-2-4-14-spokelsesbronnen-article9138-1094.html

Remen, A. (1991). Flow and Shallow Gas Evaluation. *2/4-14 Experience Transfer Seminar*.

Schlumberger. (2018, May). *Schlumberger Oilfield Glossary*. Retrieved from Schlumberger : http://www.glossary.oilfield.slb.com/Terms/r/refraction.aspx

xsgeo. (2018, January). *Frequency filtering in practice.* Retrieved from xsgeo: http://www.xsgeo.com/course/filt.htm#poststack

Zadeh, H. M., & Landrø, M. (2011, January). Monitoring a shallow subsurface gas flow by time-lapse refraction analysis. *GEOPHYSICS 76(6), O35-O43*.

Appendix A

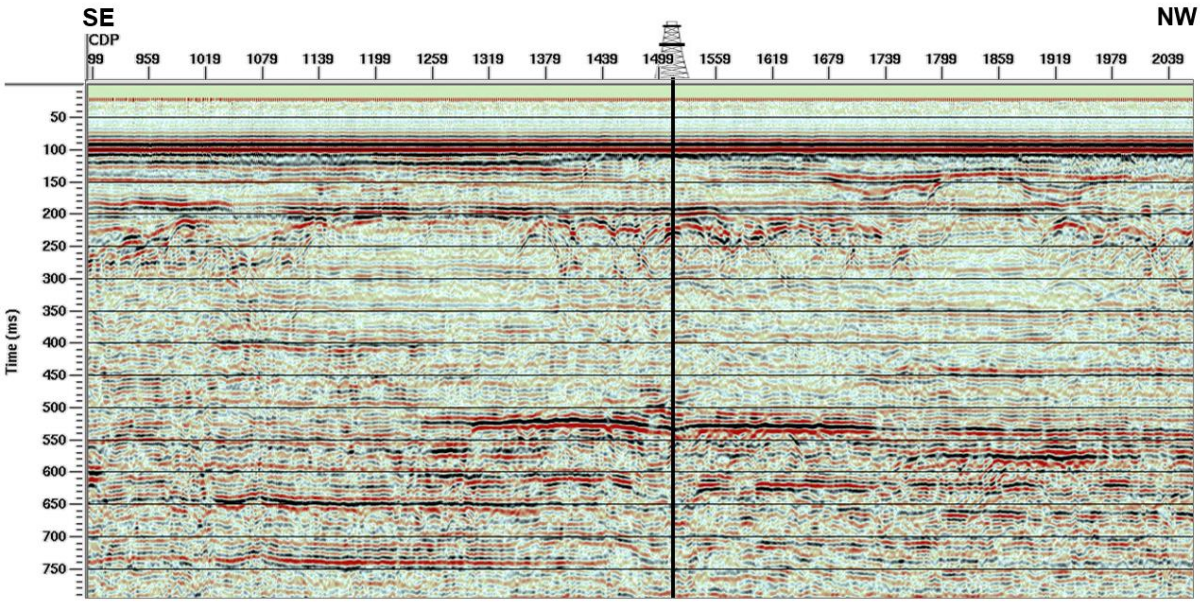

A 1: *Stack of 2009 data. The well is marked with a black line. Orientation is from southeast to northwest along line 804.*

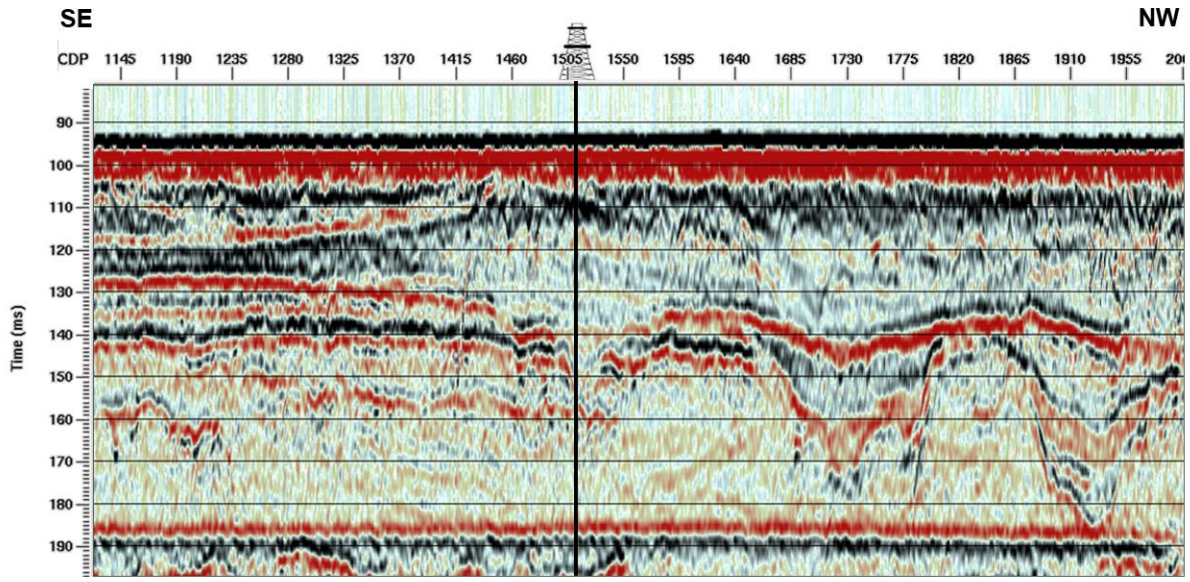

A 2*: Closeup of the stack from 2009, displaying the upper 197 ms. The tunnel valleys are clearly visible from approximately 130 to 170 ms. The well is marked in a black line at CDP 1514.*

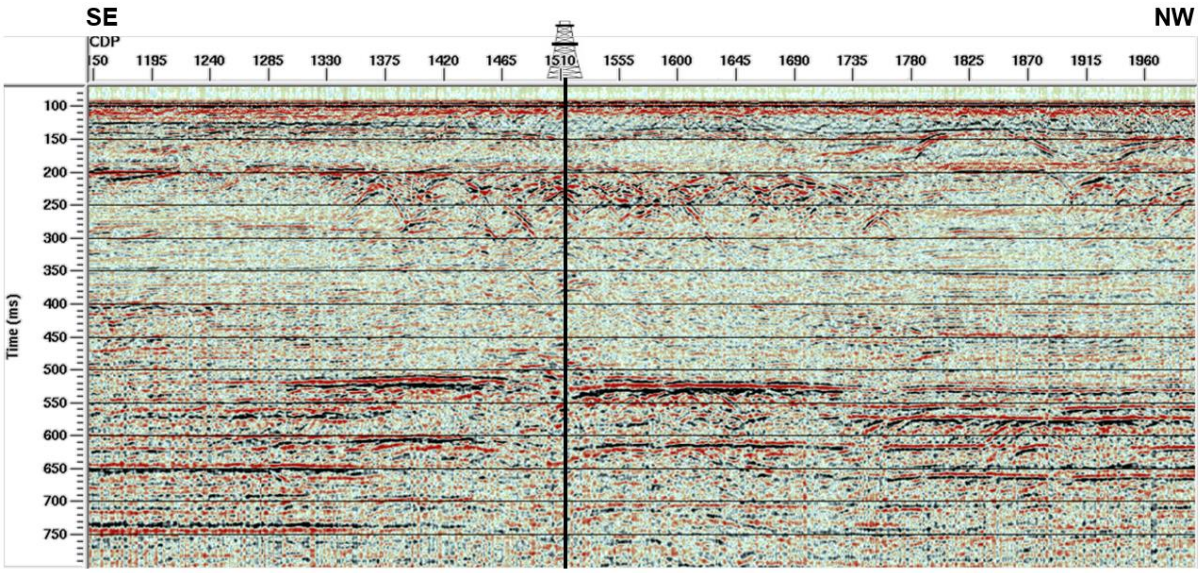

A 3: *Difference stack of the 2009-1990 data. The well is marked with a black line. Orientation is from southeast to northwest along line 804.*

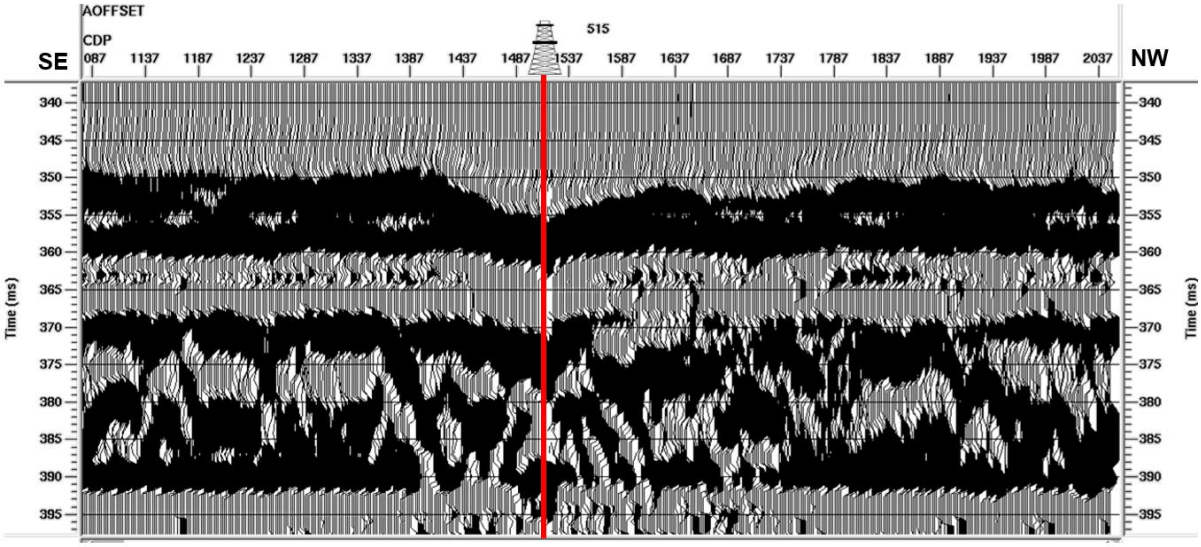

A 4: *Trace from 1990 data at offset 515 for each CDP gather along line 804. Well 2/4-14 is indicated with a red line at CDP 1514. The sail line direction is from southeast to northwest. The first event intersecting shows an increase in travel time intersecting the well, and further northwest at approximate CDP location1387 to 1737 another increase occurs*

Appendix B

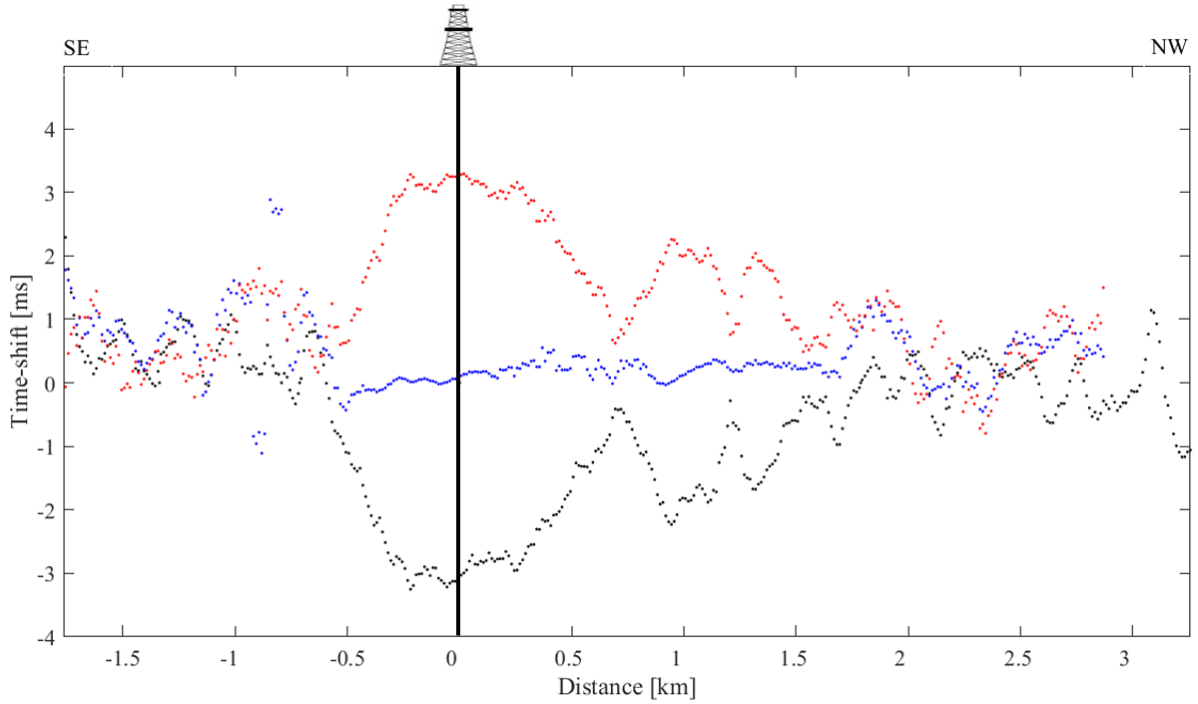

B 1: *Cross-correlation of all three datasets at offset 515 m. No smoothing function or interpolation is applied.*

Appendix C

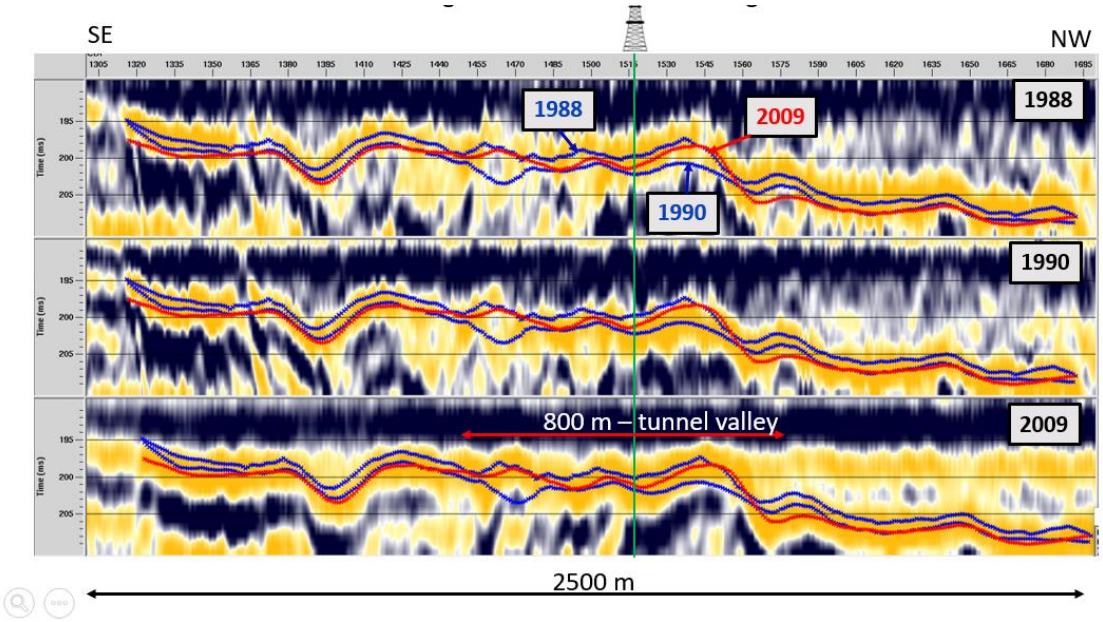

C 1: *Shallow time-shifts showing indications of leakage pattern. Alignment of seabed reflection to 100 ms. Near to the well: significant increase in time-shift between 88 and 90 – followed by a reduction back to pre-blowout values again – 800 m width. Outside this region, the situation is unchanged between 1990 and 2009. Work by Martin Landrø.*

C 2: *Picture taken 9 December 1989. A few gas bubbles close to 2/4-13, 47 m away from the blowing well. (Landrø M. , 2014)*